Accepted Manuscript

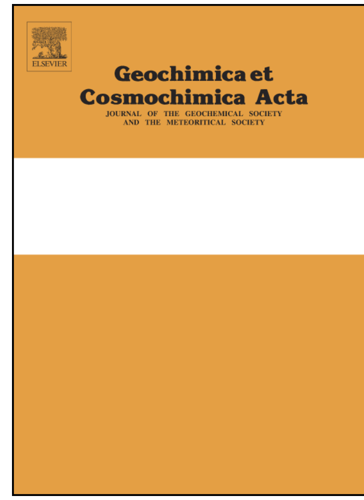

The weathering of micrometeorites from the Transantarctic Mountains

Matthias van Ginneken, Matthew J. Genge, Luigi Folco, Ralph P. Harvey

PII: S0016-7037(16)30001-1
DOI: http://dx.doi.org/10.1016/j.gca.2015.11.045
Reference: GCA 9592

To appear in: *Geochimica et Cosmochimica Acta*

Received Date: 20 January 2015
Accepted Date: 25 November 2015

Please cite this article as: van Ginneken, M., Genge, M.J., Folco, L., Harvey, R.P., The weathering of micrometeorites from the Transantarctic Mountains, *Geochimica et Cosmochimica Acta* (2016), doi: http://dx.doi.org/10.1016/j.gca.2015.11.045

The weathering of micrometeorites from the Transantarctic Mountains

Matthias van Ginneken[a,b*], Matthew J. Genge[a], Luigi Folco[c], Ralph P. Harvey[d]

[a]IARC, Department of Earth Science and Engineering, Imperial College London, Exhibition Road, London SW7 2AZ, UK

[b]Department of Earth Sciences, The Natural History Museum, Cromwell Road, London, SW7 5BD, UK

[c]Dipartimento di Scienze della Terra, Università di Pisa, Via S. Maria 53, 56126 Pisa, Italy

[d]Department of Geological Sciences, 112 A. W. Smith Building, Case Western Reserve University, Cleveland, Ohio 44106–7216, USA

*Corresponding author. E-mail: m.van-ginneken@imperial.ac.uk

Abstract

Micrometeorites are cosmic dust particles recovered from the Earth's surface that dominate the influx of extraterrestrial material accreting to our planet. This paper provides the first in-depth study of the weathering of micrometeorites within the Antarctic environment that will allow primary and secondary features to be distinguished. It is based on the analysis of 366 particles from Larkman Nunatak and 25 from the Transantarctic Mountain collection. Several important morphological categories of weathering effects were identified: (1) irregular and faceted cavities, (2) surface etch pits, (3) infilled cavities, (4) replaced silicate phases, and (5) hydrated and replaced metal. These features indicate that congruent dissolution of silicate phases, in particular olivine, is important in generating new pore space within particles. Comparison of the preservation of glass and olivine also indicates preferential dissolution of olivine by acidic solutions during low temperature aqueous alteration. Precipitation of new hydrous phases within cavities, in particular ferrihydrite and jarosite, results in pseudomorph textures within heavily altered particles. Glass, in contrast, is

Abbreviations: LK = Larkman Nunatak; TAM = Transantarctic Mountains.

altered to palagonite gels and shows a sequential replacement indicative of varying water to rock ratios. Metal is variably replaced by Fe-oxyhydroxides and results in decreases in Ni/Fe ratio. In contrast, sulphides within metal are largely preserved. Magnetite, an essential component of micrometeorites formed during atmospheric entry, is least altered by interaction with the terrestrial environment. The extent of weathering in the studied micrometeorites is sensitive to differences in their primary mineralogy and varies significantly with particle type. Despite these differences, we propose a weathering scale for micrometeorites based on both their degree of terrestrial alteration and the level of encrustation by secondary phases. The compositions and textures of weathering products, however, suggest open system behaviour and variable water to rock ratios that imply climatic variation over the lifetime of the micrometeorite deposits.

1. Introduction

Micrometeorites are extraterrestrial particles 10 μm to 2 mm in size, which represent in term of mass the most important part of the flux of extraterrestrial material to accrete to the Earth's surface (Rubin and Grossman, 2010). The particularly dry and cold conditions and low abundance of atmospheric contaminants make Antarctica an ideal location for the preservation and recovery of this extraterrestrial material. Over the last decades, numerous micrometeorite collections have been obtained: by melting ice in the South Pole Water Well station (Taylor et al., 1998), the Cap Prud'homme station (Maurette et al., 1991), and in the Yamato Mountains (Terada et al., 2001); by melting of fresh snow in Concordia station (Duprat et al., 2007); by processing sediments on top of nunataks in the Transantarctic Mountains (TAM) (Rochette et al., 2008). Micrometeorites have also been successfully extracted from a glacial moraine at the Larkman Nunatak in 2006. Micrometeorites collected from ice and snow have generally young terrestrial ages, as they were collected only in the younger superficial layers (up to ~10 ka for the South Pole Water Well collection; Taylor et al., 1998). On the other hand, micrometeorites from the TAM have accumulated over the last ~1 Ma (Folco et al., 2008; Rochette et al., 2008).

Studies have shown that Antarctic meteorites have suffered chemical weathering despite being preserved in the Earth's driest and coldest environment. The effects of weathering on Antarctic meteorites have been extensively described in the literature (Gooding, 1982; Gooding, 1986a; Gooding, 1986b; Velbel, 1988; Jull et al., 1988; Velbel and Gooding, 1990; Velbel et al., 1991; Wlotzka, 1993; Bland et al., 2006; Losiak and Velbel, 2011; Velbel, 2014). They include rusting of metallic phases to Fe-oxyhydroxides, hydrolysis of silicates and formation of clay minerals, and precipitation of evaporitic carbonates and sulphates. During weathering, elements are mobilized and are either gained or lost depending on the chemistry of the material in which they were stored or on the mineralogy of the meteorite (Bland et al., 2006). Weathering scales for ordinary chondrites and CR and CK carbonaceous chondrites have been developed and are based on the progressive replacement of primary phases by weathering products (Wlotzka, 1993; Rubin and Huber, 2005). Due to significant differences in mineralogy and chemistry between meteorite groups, developing a unique scale of weathering for all meteorites is not possible.

Although effects of weathering on micrometeorites have been mentioned in the literature, explaining the geochemical processes producing them was not the principal objectives of these works (Blanchard et al., 1980; Genge and Grady, 1998; Blackhurst et al., 2004; Suavet et al., 2009; Van Ginneken et al., 2012; Taylor et al., 2012). The preferential dissolution of silicate minerals is a terrestrial weathering effect observed in collections from the deep-sea, Greenland, the South Pole Water Well, and the TAM (Blanchard et al., 1980; Maurette et al., 1987; Suavet et al., 2009; Taylor et al., 2012). Other effects of weathering include COPS phases (for Carbon-, Phosphorous- and Sulphur-bearing iron oxides) resulting from the oxidation of metallic phases (Genge and Grady, 1998; Blackhurst et al., 2004). The overabundance of magnetite dominated particles (I-type and G-type cosmic spherules) from the deep-sea, which are more resistant to weathering than silicate-dominated particles, shows that terrestrial weathering can introduce an important bias in micrometeorite collections. Therefore, knowing how terrestrial weathering will affect the preservation of micrometeorites and evaluating possible biases introduced in large micrometeorite collections can have a significant impact for studies focusing on the estimation of the flux of extraterrestrial matter to the Earth's surface. This is especially the case for old collections, which can give important information on the variability of this flux over the recent geological past (e.g., the TAM collection; Rochette et al., 2008).

Here, we report the first comprehensive study of the weathering of micrometeorites from the Larkman Nunatak (hereafter LK), Antarctica. Micrometeorites from the TAM collection are also studied for comparison. The main aim of this work is to describe the effects of terrestrial weathering on micrometeorites and the geochemical processes controlling them. We will then discuss the implications of this work for the determination of weathering rates of micrometeorites, the effects of weathering for the preservation and abundance of micrometeorites, and the environmental factors controlling the weathering of micrometeorites. Finally, we will present the first weathering scale for micrometeorites from Antarctica.

2. Samples and methods

2.1. Sample selection

The micrometeorites studied in this work were recovered from a glacial moraine near LK (85° 46'S, 179° 23' E). Micrometeorites from LK were collected in 2006 by one of us

(MG), whilst those from the TAM collection were collected during the 2006 Programma Nazionale di Ricerche in Antartide (PNRA) expedition. The LK micrometeorites were collected within moraine beneath a 4 cm thick snow cover (Fig. 1). The moraine is an East-West plateau extending ca. 1.5 km by 700 m, which rises up to 30 m above the surrounding meteorite-rich blue ice. It is separated from the nunatak by a depression of up to 500 m wide. Samples were collected from the southern edge of a boulder ridge approximately 40 m into the moraine and located approximately half way through the moraine along an East-West traverse. Bedrock exposed at LK is restricted to thick lava flows of the Kirkpatrick basalt with well-developed columnar jointing evident on larger exposures. Extensive hydrothermal alteration of the basalt has occurred in places, with abundant amygdales filled with zeolites and calcite. Within the moraine, basalt also represents the most abundant lithology amongst larger boulders. However, a diverse assemblage of lithologies is present, including pale ochre calcareous siltstones, micritic limestones, dolerite, and sparse anthracitic coal. Siltstones tend to form tabular clasts due to extraction along bedding and include abundant well-preserved fossil ferns. Silicified to carbonised fossil wood is also present in these rocks. A layer of fine-grained material ranging in size from clay to 5 cm granules was present throughout the snow covered areas of the moraine at the margin between the snow and the underlying blue ice. Reverse grading was noted in the fine-grained layer. Samples were collected from the fine-grained layer.

Micrometeorites from the TAM collection were recovered from traps at the top surface of the Miller Butte (72°42.078’ S, 160°14.333’ E) and Pian delle Tectiti (74°11.013' S, 162°14.375' E) nunataks (MB and PT in Fig. 1). Detailed information on the collection procedure is given in van Ginneken et al. (2012). The geological settings of Miller Butte and

Pian delle Tectiti were described by Van Ginneken et al. (2010) and Folco et al. (2008, 2009), respectively.

The moraine samples were prepared by washing in water and were subsequently dried and size separated using 106, 250, 425 and 850 µm sieves. Three hundred and eighty-eight micrometeorites >106 µm in size were hand-picked from the sieved material under the stereomicroscope. Micrometeorites were identified on the basis of their shape (e.g., cosmic spherules) and dark colour. In addition, 25 micrometeorites from the TAM collection held at the Museo Nazionale dell'Antartide, University of Siena, Italy, were studied and selected specifically for their weathering effects.

2.2 Petrography and major element analyses

The micrometeorites were first mounted on clear adhesive tape and observed using a LEO 1455 environmental scanning electron microscope (SEM) at the Imaging and Analysis Centre (IAC) of the National History Museum (NHM) London, to gather information on morphology and structure. Subsequently, the micrometeorites were embedded in epoxy, sectioned and polished at the NHM. A petrographic study of the sectioned micrometeorites was carried out using a Zeiss EVO 15LS SEM and a Philips XL30 field-emission SEM.

Micrometeorites were analysed by wavelength dispersive X-ray (WDX) spectrometry using a Zeiss EVO 15LS SEM at the IAC. Operating conditions were an accelerating voltage of 15 kV, a 3.0 nA beam current, and a beam spot of 4 µm. Cobalt metal and Kakanui augite were used for instrumental calibration. Both S and C could be detected by the detector. Detection limits (and standard deviation) for the determined oxides (data in wt.%) are as follows: Na_2O = 0.01 (±0.09), MgO = 0.15 (±0.14), Al_2O_3 = 0.07 (±0.10), SiO_2 = 0.27 (±0.19), P_2O_5 = 0.04 (±0.03), SO_3 = 0.01 (±0.06), Cl = 0.02 (±0.04), K_2O = 0.02 (±0.06), CaO = 0.12 (±0.06), TiO_2 = 0.01 (±0.07), Cr_2O_3 = 0.01 (±0.03), MnO = 0.01 (±0.03), FeO = 0.13 (±0.16), NiO = 0.12 (±0.05). Minor and major elements represent elements having a concentration below and above ~1 wt.%, respectively.

2.3. Fourier transform infrared spectroscopy

Fourier transform infrared (FTIR) spectroscopy spectra of four cosmic spherules were determined using a Philips PU9800 FTIR spectrophotometer at the NHM. A 50x50 µm aperture was used and the spectra are averages of 40 individual analyses each. Both pristine and altered areas of cosmic spherules were analysed in the Mid-Infrared (8 to 15 µm) with a step increment of 2 cm^{-1}.

3. Results

3.1. Micrometeorites studied

Table 1 lists all the micrometeorites studied; they have been classified using the scheme by Genge et al. (2008). This classification scheme is based on the degree of thermal alteration suffered during atmospheric entry heating. For this study, micrometeorites of four different classes were studied, including the totally melted cosmic spherules, the partially melted scoriaceous micrometeorites and the fine-grained and coarse-grained unmelted micrometeorites.

Cosmic spherules are subdivided into three types: S-type, G-type and the I-type cosmic spherules. S-type cosmic spherules are mainly made of silicate phases, such as olivine and glass. G-type cosmic spherules comprise magnetite dendrites embedded in glass. Finally, I-type cosmic spherules are dominated by magnetite and wüstite, with rare FeNi metal inclusions. S-type cosmic spherules are further subdivided into six subtypes sorted by increasing peak temperature experienced during atmospheric entry heating: the CAT cosmic spherules, mainly composed of refractory elements; the V-type cosmic spherules consisting mainly of glass; the cryptocrystalline (CC) cosmic spherules dominated by submicrometer crystals of olivine and magnetite; the barred olivine (BO) cosmic spherules dominated by parallel growths of olivine crystals within glass; the porphyritic olivine (Po) cosmic spherules dominated by equant and skeletal olivine within glass; and, finally, the coarse-grained cosmic spherules, which contain more than 50 volume % of relict minerals.

The scoriaceous micrometeorites consist of fayalitic olivine microphenocrysts with interstitial glass. They often contain abundant relict mineral phases and relict matrix areas. The fine-grained unmelted micrometeorites have a texture and mineralogy similar to C1, C2 and C3 carbonaceous chondrite matrix. The coarse-grained micrometeorites can be chondritic or achondritic. In this study, we have only studied chondritic coarse-grained micrometeorites having a texture and mineralogy similar to equilibrated ordinary chondrites.

3.2 Identifying potential weathering features

Potential mineralogical and textural properties in micrometeorites formed as a result of terrestrial weathering are distinguished from primary features formed during atmospheric entry heating on the basis of several criteria: (1) spatial correlation with the surface of particles or individual crystals, (2) voids that may be formed by dissolution of pre-existing phases, and (3) partial to complete fillings of irregular voids or vesicles with polycrystalline assemblages of minerals. These criteria provide strong evidence for an origin by weathering within particles that experienced melting during atmospheric entry and that are unlikely to preserve mineralogical or textural evidence for parent body aqueous alteration (i.e., alteration on the source asteroid or comet). In unmelted fine-grained micrometeorites these criteria provide only weak evidence for origin by terrestrial weathering. These considerations will be discussed further later in interpreting weathering effects.

3.3. Categories of weathering effects

Several distinct categories of weathering effects were observed within particles in the current study and vary widely in intensity with particle type and between individual particles. The most important weathering effects are: (1) irregular or faceted cavities, (2) etch pits, (3) infilled cavities, (4) replaced silicate phases, and (5) hydrated and replaced metal.

Irregular and faceted cavities

As a general rule, cavities are identified in micrometeorites by their extremely low signal intensity in BSE images in comparison to mineral phases. In BO, Po and CC cosmic spherules, the cavities occur mainly within olivine crystals. Identical cavities have already been observed in micrometeorites from Antarctica and from deep sea sediments (Blanchard et al., 1980; Brownlee et al., 1997; Suavet et al., 2009). Cavities showing irregular shapes typically occur within olivine crystals (e.g., Fig. 2a), whereas faceted cavities are devoid of remnant olivine and are bordered by interstitial glass and are typically present in BO and Po cosmic spherules (e.g., Figs. 2b-f). The faceted cavities show euhedral or elongated shapes similar to coexisting olivine crystals. In BSE images of CC cosmic spherules, cavities are characterized by their shape, which are similar to skeletal crystals of olivine, whereas the interstitial glass has been preserved (e.g., Figs. 3a and 3b). In partially weathered cosmic spherules, the cavities are concentrated on the margins of the particles and are often absent in their core area (Figs. 2a and 2d-i). In CC cosmic spherule #LK06-0091, cavities are also concentrated along a crack cutting through the particle (Fig. 2h). In general, the size of the cavities ranges from several tens of µm to below the resolution of a SEM. In most cases, the cavities are devoid of secondary materials (e.g. Figs. 3c-f).

Irregular and faceted cavities were observed in 41% of the Po cosmic spherules from LK. The abundance of cavities varies between individual particles and represents up to 100% of the crystalline phases in particles (i.e. excluding interstitial glass). In BO cosmic spherules, 49% of the particles exhibit cavities to a various extent.

Etch pits

Etch pits were observed in 13 Po cosmic spherules from LK (Figs. 3c and 3f). Their V-shaped outline is identical to etch pits observed in terrestrial olivine (Velbel, 2009, and references therein). The etch pits commonly occur simultaneously with irregular and faceted cavities.

In cross-section, etch pits are wedge-shaped and parallel to each other. The etch pits typically occur in euhedral olivine crystals and are identified by their low signal intensity in SEM-BSE images. Etch pits also occur in olivine crystals of coarse-grained unmelted micrometeorite #20c.343 (Fig. 4a). Rarely, two triangular etch pits can share a base, consequently appearing as diamond-shaped in cross-sections of olivine crystals (e.g., Figs. 3c and 3f). The sizes of the etch pits are highly variable within individual olivine grains but are generally smaller than 10 µm. The etch pits are devoid of secondary material.

Infilled cavities

Some rare cavities in micrometeorites are partially to completely filled with fine-grained mineral assemblages. Figures 2h, 2i, 3b and 3e show BSE images of CC and BO cosmic spherules. These particles exhibit both empty cavities, which are illustrated by their low signal intensity in BSE images, and infilled cavities which are mainly concentrated on the margins of the particles and along cracks cutting through the particles. Crystals of jarosite were also observed lining a rounded vesicle ~20 µm in size in altered BO cosmic spherule #LK06-0526 (Fig. 3g; Table 2). Apart from jarosite, the infilling material in other cosmic spherules does not show any recognizable structure at the micrometer-scale. Jarosite is also present as weathering products in scoriaceous micrometeorite #6.19 (Fig. 5c), filling up the smallest vesicles and as large (≥10 µm) euhedral crystals on the fringe of practically every other large vesicle. Jarosite is observed in negative crystals of olivine in unmelted micrometeorites #20c.343 and #20c.344 (Table 2). For particles #7bis.03, #21p.05 and #20b., the secondary products appear to be a mixture of a sulphate (likely jarosite) and possibly clay minerals.

Table 3 shows the major element composition of the material filling negative crystals of olivine in CC cosmic spherules #LK06-0044, #LK06-0091, #20.02 and in the BO cosmic spherule #18c.01. Note that for these cosmic spherules the spot size used for these analyses is larger than the maximum size of the pseudomorphs analysed, so compositions are likely a mixture of secondary infilling material and interstitial glass. The total of the analyses is low and ranges from 81.2 to 86.3 wt%. Infilling material is consistently Si and Fe-rich (14.8 – 37.2 wt% SiO_2; 24.0 – 31.2 wt% Fe_2O_3). Lesser amounts of Al are recorded but are broadly constant (5.98 – 6.53 wt% Al_2O_3). In #LK06-0091, Ca concentration is high (5.55 wt% CaO) and S and Cr have low concentrations (2.70 wt% SO_3; 1.01 wt% Cr_2O_3). In #LK06-0044, #20.02 and #18c.01, other concentrations are broadly similar, with high S (18.2 – 26.8 wt% SO_3), appreciable amounts of K (4.86 – 7.11 wt% K_2O), and minor Ca and Mg (0.63 – 1.23 wt% CaO; 0.50 – 0.90 wt% MgO).

Infilled cavities have also been observed in scoriaceous and coarse-grained unmelted micrometeorites (Figs. 4b, 5a- d). In scoriaceous micrometeorites #LK06-0085 and #LK06-

0074, some vesicles are encrusted with Fe-oxide (close ups of Figs. 5a and 5b). In #20c.344, infilled cavities are characterized by their relatively limited size (<20 µm) and subrounded shape (close-up of Fig. 5c). Element maps of coarse-grained unmelted micrometeorites #19b.13 and #19b.25 (Figs. 4b1 and 4d1, respectively) and major element compositions of the infilling material (Table 3) show that cavities are filled with Fe-oxide/oxyhydroxide. Element maps of #20c.343, #19b.13, #19b.24 and #19b.25 also show that although jarosite (light blue in Figs. 4a2, 4b2, 4c2 and 4d2) does not entirely fill up cavities, it frequently lines them.

FTIR data from cosmic spherules #LK06-0091, #20.02 and #20.01 are reported in Fig. 6. IR spectra were determined for both unaltered and altered areas of the particles. Spectra 1, 3 and 5 of pristine areas of the three particles show bands typical of olivine (Morlok et al., 2006). Spectrum 2 of the altered margin of #LK06-0091 shows very low reflectance and broad bands that are not easily identifiable, although one is visible at 10.00 µm. Spectra 4, 6 and 7 of altered areas of #20.02 and #20.01 show bands at ~9.10 µm and ~10.00 µm, which can be attributed to the ν3 sulphate bending mode and δOH band in jarosite (Bishop and Murad, 2005).

Replaced silicate phases

Glass is a major phase in S-type cosmic spherules, and is virtually the only observable primary phase in V-type cosmic spherules (Genge et al., 2008). The composition of pristine glass in the studied V-type cosmic spherules has a typical chondritic composition (Table 4; Cordier et al., 2011). Figures 2j to 2l show SEM BSE images of the three V-type cosmic spherules #LK06-0036, #LK06-0119, and #LK06-0116, respectively. These particles are characterized by areas on their outer parts showing lower signal intensity in BSE images compared to the rest of the particle. Such “dark” areas have been observed in 42 V-type cosmic spherules to various extents. Similar dark areas have been observed on V-type cosmic spherules from the South Pole Water Well collection (Taylor et al., 2012). Three types of dark areas have been observed: (1) pits of various sizes scattered on the surface of the particle (Fig. 2j); laminations (Fig. 3h) and microcracks are observed in the pits, whereby the latter are radial or parallel to the surface of the particles; (2) a lamellar discontinuous layer on the surface of the fresh glass (Figs. 2k and 3i). The boundary layer between the dark area and the pristine glass is irregular and the geometry of the laminations is not continuous and is similar to what is observed in the pits described previously; and (3) A continuous layer totally surrounding the particles (Figs.2l and 3j). The thickness of the layer is constant and laminations are frequently observed parallel to the original surface of the particle. All but one particle from the TAM collection show pits only. In all cases, weathering features are observed in the outer part of the spherules and fresh glass is still present in the core of the particles.

Table 4 shows the major element composition of pristine glasses and altered layers in 27 V-type cosmic spherules from the LK collection and 13 from the TAM collection. Totals in corrosion products are low, ranging between 64.2 and 83.8, suggesting that they contain a hydrous component. FTIR data for the two partially altered V-type cosmic spherules #7.40 and #21p.1 from the TAM collection are shown in Figure 7. Particle #21p.1 is characterized by a lamellar discontinuous layer surrounding the particle. Particle #7.40 shows more complex weathering features, with one side of the particle dominated by cracks filled with jarosite (Table 2). In both particles, the IR spectra of the pristine glass feature two broad bands at ~10 and ~12 µm (Fig. 7). The spectra of altered glass show a main sharper band at ~9.2 µm. In the altered glass, shoulders are also observed between 8 and 9 µm and 10 and 12 µm. In the spectra 2 and 3 of particle #7.40 a sharp band is also observed at ~10 µm, which can be attributed to jarosite that is abundant in the area analysed.

Hydrated and replaced metal and sulphide

Metallic phases are rare in micrometeorites and mainly appear as FeNi metal (Genge et al., 2008). In S-type cosmic spherules, metal droplets are made of FeNi metal and/or sulfides and are usually observed on the outer rim of the particles (Genge and Grady, 1998). In G-type and I-type cosmic spherules, which are essentially made of dendrites of magnetite within interstitial glass and an assemblage of magnetite and wüstite, respectively, FeNi metal is sometimes observed as spheres inside the particles (Brownlee et al., 1997; Genge et al., 2008; Rudraswami et al., 2014). In scoriaceous micrometeorites, FeNi metal occasionally occurs with or without sulphide (FeS) in metal droplets in cosmic spherules, which may have formed as immiscible metallic/sulphide liquids during atmospheric entry heating (Genge et al., 2008). Metal and sulphide constitute an accessory phase of unmelted micrometeorites, with textures similar to those observed in ordinary chondrites in the case of the coarse-grained unmelted micrometeorites from the TAM (Van Ginneken et al., 2012).

Droplets of FeNi metal and sulphide were observed in 11 S-type cosmic spherules from the LK collection (Fig. 8). The major element composition of some FeNi metal and sulphide is reported in Table 5. In all samples, the Ni content ranges between 10.7 and 53.2 wt%. The composition of the sulphides is non-stoichiometric and consists broadly of a mixture of Fe-S-Ni. In 9 S-type cosmic spherules, FeNi metal is associated with Fe-oxide (Fig. 8). Similar Fe-oxide has been observed partially to totally replacing FeNi metal and sulphide on the margin of S-type cosmic spherules from Antarctica (Engrand et al., 1993; Blackhurst et al., 2004). Even if the amount of Fe-oxide is greater than 50 vol%, the original textures and outlines of the metal droplets are preserved (e.g., Figs. 8c, 8d, 8g and 8h). The major element composition of Fe-oxide is reported in Table 6. Although the composition of Fe-oxide may vary widely from one particle to another, Fe remains the main component (47.5 – 70.0 wt% Fe_2O_3). Other major elements are S, Ni and Si (4.59 – 9.79 wt% SO_3; 0.94 – 8.72 wt% NiO; 4.02 – 10.3 wt% SiO_2). Other elements include Al, Ca and occasionally Na and Mg. Chlorine occurs in Fe-oxides of 8 particles. The low totals of the analyses of these oxides (78.2 – 88.4 wt%) imply they are hydrated oxides (e.g., oxyhydroxides). Laminated oxides of identical composition and texture are also observed encrusting the former metal droplets and forming a continuous rim up to about 20 µm. Based on BSE images, it is not clear if the oxides are crystalline or amorphous. Magnetite dendrites are observed on the margins of the hydrated Fe-oxide in particle #LK06-0074 (Fig. 8h).

Spheres of FeNi metal were observed in 6 I-type cosmic spherules and in G-type cosmic spherule #LK06-0027 from the LK collection. In the 6 I-type cosmic spherules, FeNi metal is the only constituent of spheres that are completely surrounded by magnetite and/or wüstite (Fig. 2n). The G-type nature of #LK06-0027 is suggested by the dendritic nature of its magnetite and by the presence of interstitial Fe-rich silicate (Figs. 2o and 3l). In #LK06-0027, a sphere consisting mainly of Fe-oxide is enclosed in the pristine magnetite (Fig. 3l). This sphere is partially exposed to the surface of the particle. As in the S-type cosmic spherules, the part of the sphere exposed at the surface is encrusted by a laminated Fe-oxide (Fig. 2o). Some cracks cutting through the magnetite/silicate part of the particle and radiating from the metal/oxide sphere are also observed. The major element compositions of the oxides, of the material filling, the crack and of the encrustations are reported in Table 7.

4. Discussion

4.1. The weathering of the main mineral phases in micrometeorites

4.1.1. Olivine

Olivine is the major constituent of BO, Po, CC, and coarse-grained cosmic spherules, as well as and of scoriaceous micrometeorites (Genge et al., 2008). It is well documented that olivine is one of the least stable silicate minerals on the Earth's surface, and as a consequence is one of the most sensitive to chemical weathering (e.g., Delvigne et al., 1979; Nesbitt and Wilson, 1992; Bland and Rolls, 1998; Stefánsson et al., 2001). Chemical weathering is mainly controlled by temperature and the availability of liquid water, but even in the case of the hydrocryogenic (i.e., presence of limited quantity of liquid water below freezing temperature) and arid conditions encountered on the ground surface of Antarctica, olivine remains particularly sensitive to chemical weathering (Gooding, 1986a). In 117 BO, Po, CC and coarse-grained cosmic spherules from the LK and TAM collections, olivine crystals suffered partial to total dissolution, as indicated by the irregular and faceted cavities observed within these particles (Figs.2a-i). Furthermore, FTIR data of #LK06-0091 (BO), #LK06-0091 (CC) and #20.02 (CC) show that in pristine areas typical bands for olivine are clearly visible, whilst in altered areas, olivine bands are absent suggesting complete removal (Fig. 6). Dissolution of olivine crystals is also observed in scoriaceous micrometeorites #LK06-0095, #LK06-0096, and to a greater extent in #20c.344 and #6.19 (Fig.5). Amongst coarse-grained unmelted micrometeorites, #20c.343 and #19b.13 exhibit dissolved olivine crystals at their margins (Fig. 4). The absence of alteration products in most dissolved olivine grains suggest that congruent dissolution occurred. The loss of Fe^{2+}, Mg^{2+} and silica by congruent dissolution of olivine usually happens in acidic water (Burns, 1993). The concentration of dissolved olivine grains towards the surface of particles suggests that dissolution is the result of surface correlated weathering.

The presence of wedge-shaped etch pits along the faces of partially dissolved olivine crystals (e.g., Figs. 3c, 3f and 3k) in 13 Po cosmic spherules and in the coarse-grained unmelted micrometeorite #20c.343 suggest low-temperature chemical weathering of olivine in the terrestrial environment (Velbel, 2009). The homogeneous morphology of etch pits and their orientation parallel to one another is different to biotic corrosion features observed in some terrestrial basalts and mantle rocks (i.e., irregular tunnels rarely parallel to one another; Fisk et al., 2006). This suggests that dissolution of olivine in Antarctic micrometeorites occurs in an abiotic environment. The preferred orientation of pits is likely to be controlled by the crystallographic orientation of olivine grains (Lee et al., 2013).

4.1.2. Glass

Structures identical to the corrosion pits, and discontinuous and continuous altered layers described in section 3.3 were observed on stained glass windows from the Middle Ages (Sterpenich and Libourel, 2001). The morphology and thickness of these three structures is controlled by different types of weathering, with corrosion pits being driven by moisture (i.e., very low water/rock ratio), discontinuous layers by atmospheric weathering (i.e., direct exposure to rainfalls; intermediate water/rock ratio) and continuous layers by weathering by constant contact with groundwater (i.e., highest water/rock ratio). The similarity in textures between cosmic spherules and artificial glass weathering products suggest that alteration features observed in V-type cosmic spherules are the result of hydration and leaching of the surface of the glass during aqueous alteration.

Chemical analyses of altered areas have low totals (≤80 wt%), which can be attributed to the presence of water. We suggest that these different structures of alteration in V-type cosmic spherules are controlled by variations in water availability. Observation of two types of weathering affecting individual particles suggest that weathering conditions may not have been stable during the storage of the particles in the LK moraine with variations in the water/rock ratio suggesting fluctuations in water influx presumably due to climatic conditions. Another possibility is a change of microenvironment, and thus of water/rock ratio, if the particle may have moved in the moraine over time.

The composition and infrared spectra of the alteration products on V-type cosmic spherules suggest that they consist of a palagonite-like gel. Palagonite is a complex assemblage of clays and amorphous material at the submicrometer scale resulting from the alteration of basaltic glass (e.g., Stroncik and Schmincke, 2002). FTIR data of particles #21p.1 and #7.40 are consistent with observations in artificially corroded SiO_2-rich glass (Sanders and Hench, 1973). IR spectra are, thus, consistent with the production of a palagonite-like gel forming as weathering of V-type cosmic spherules progresses.

The main difference between the alteration of natural basaltic glasses and glass in V-type cosmic spherules is that as weathering progresses in the former, several additional layers of poorly to very crystalline material form. Crovisier et al. (1992) studied subglacial volcanic glasses from Iceland and observed that palagonite formation is followed by the formation of an external layer made of clay minerals having a smectite-like structure. This sequence of alteration was observed in samples exposed to relatively stable climatic conditions (i.e., temperature and humidity). In a sample exposed to high fluctuation of temperatures and to more contrasted humidity, only an amorphous alteration product was observed. Crovisier et al. (1992) explained that under high humidity conditions the alteration progresses slowly and clay minerals will tend to be unstable, whereas under low humidity conditions the alteration progresses quickly, leading to the formation of clay minerals. They argued that with such variable conditions, the proto-mineral structures cannot be efficiently reorganized. Similar processes may explain the lack of crystalline material in V-type cosmic spherules, as they are exposed to variable weathering conditions in the Antarctic moraine.

Mass-balance calculation

The lack of correlation between the original glass composition and that of the alteration products suggests open system behaviour with transport of components as solvents away from the site of weathering. The behaviour of elements during alteration of the glass can be addressed by calculating the mass balance between pristine glass and altered glass. For mass-balance calculation, the isocon method was used (Grant, 1986; Grant, 2005). This method was preferred because it does not require significant data manipulation and can be accomplished both graphically and numerically to determine changes in volume, mass or element concentration during metasomatism. Based on Grant (2005), the equation for composition – volume relations is written as

$C_i^A = (M^O/M^A)(C_i^O+\Delta C_i)$ (1)

where Ci is the concentration of the element "i", "A" refers to the altered sample, "O" refers to the original sample, and M is equivalent mass before and after alteration. ΔC_i is the change in concentration of the species "i" during alteration. If change in density during alteration is known, it is then possible to analyse the mass balance using

$M^O/M^A = \rho^O V^O/\rho^A V^A$ where $M^O/M^A = \rho^O/\rho^A$ (2) assuming the volume is constant

And, thus, equation (1) becomes

$\Delta C_i = (\rho^O/\rho^A)C^A - C^O$ (3)

Figure 9 is the isocon diagram showing the behaviour of Al_2O_3, MgO, SiO_2, CaO and FeO during alteration. Figures 2j, 2k and 2l show that alteration does not affect the overall structure of the original particle, except for the presence of a variable number of open fractures. The presence of these open fractures suggests that a change in volume did occur during alteration, although the amount of volume change cannot be determined with any accuracy. It can be assumed that this change of volume is small, and alteration is broadly isovolumetric. The slope of the isocon (i.e. ρ^O/ρ^A) is 0.74 if densities of 2.7 g.cm^{-3} for pristine glass and 2.0 for the palagonite are used (Staudigel and Hart, 1983; Genge, 2007). We can then calculate mass-balance in V-type cosmic spherules by solving equation (3).

Element mobility during the alteration of glass

Results of the mass-balance calculations are reported in Table 8. A loss of SiO_2 between -16 and -41% is observed in LK particles - except for two particles exhibiting corrosion pits, in which SiO_2 is slightly enriched (+1% and +8%). In TAM particles, SiO_2 is equally lost (-2 to -21%) or gained (+9 to +17%). In all particles from the LK, Al_2O_3 is gained (+3 to +64%). On the other hand, Al_2O_3 is lost (-10 to -57%) in all but two TAM particles (0% and +30%). Silicon tends to be more difficult to remove than other major elements, because it is the main network-forming element in silicate glasses (i.e., the element responsible for the polymerisation of the glass). The contrasting behaviour of Si in LK and TAM particles suggest that different environmental conditions will affect the composition of the alteration product.

An almost total loss of MgO – between -89 and -99% - is observed in all particles and is most significant in particles exhibiting corrosion pits. This suggests that this element is particularly incompatible within the alteration product and soluble and mobile enough to be efficiently removed by the fluid. Crovisier et al. (1992) showed that during the first stage of palagonitisation of a subglacial volcanic glass, Mg is strongly depleted in the palagonite compared to the pristine glass. As palagonitisation progresses, Mg will then be reintroduced in an outer alteration layer to form more evolved alteration products, such as clays. Such evolved layers are absent in the alteration products of V-type cosmic spherules and perhaps suggest only transient aqueous alteration.

In particles showing corrosion pits, FeO is consistently lost (-1 to -77%) except for one LK particle that gained +19% FeO. FeO is equally gained and lost in LK particles showing a continuous layer (+13 to +27% and -9 to -27% respectively). As palagonitisation of volcanic glasses progresses, ferrous iron (Fe^{2+}) within the glass tends to be oxidized to ferric iron (Fe^{3+}) (Furnes, 1978). In alkaline aqueous fluids ferrous iron is much more mobile than ferric iron. The increase of iron in half of the continuous layers may be attributed to either a large amount of ferrous iron being oxidized to ferric iron or the leaching by a relatively less acid fluid.

In the altered glassy mesostases of particles MnO has experienced significant loss (-100%, within the constraints of analytical uncertainty). In LK particles, CaO is mostly lost (-11 to -82%) except for five particles in which it is gained (+5 to +25%). In TAM particles, CaO is almost completely lost (-72 to -100%). Table 8 shows that of the 24 LK particles studied, Na and K are gained in 14 and 21 particles, respectively. Na_2O and K_2O are gained in all TAM particles. Note that Na_2O and K_2O values were below detection limit in the pristine glass.

TiO_2 is gained in 8 LK particles and 3 TAM particles. Titanium was not detected in all LK particles and 3 TAM particles showed minor concentrations (up to 0.53 wt%). Increase in K_2O and TiO_2 in alteration products of some particles might be explained by the alteration of surrounding rocks present in the moraine and the micrometeorite traps, which contain these two elements (e.g., ilmenite for Ti and alkali feldspar for K). Enrichment in Na might be the result of dissolution of salts in the vicinity of the particles. The contamination of alteration products with elements foreign to the original cosmic spherules suggests that the alteration occurs in an open system implying temporary interconnectivity of the aqueous fluid present in the deposit at least on length scales of several grains.

The alteration of glass in olivine-bearing cosmic spherules is similar to that observed in V-type cosmic spherules in that the main alteration processes appear to be hydration and leaching of major elements. As the interstitial glass bands between the bars of olivine in BO cosmic spherules are usually thinner than the spot size used for chemical analysis, analysis of pristine and/or altered glass was not possible without matrix overlap from surrounding mineral phases. The same problem occurred with cryptocrystalline cosmic spherules. As a consequence, major element compositions of pristine and altered glass of only 4 Po cosmic spherules were determined (particles #7.42, #21.65, #LK06-0050 and #LK06-0018; Table 9). The absence of visible opened cracks or any change in morphology between the pristine and altered glass suggest that alteration is isovolumetric.

The calculated mass balance between the pristine and altered glass is shown in Table 8. For all major elements in the pristine and altered glass, moderate to severe losses are observed. SiO_2 is the least depleted element in the altered glass and CaO is the most. The sequence of leaching of the major elements from the glass is as follow: Ca>Mg≥Al>Fe. This could indicate that the solvent was slightly acidic (Banin et al., 1997), which is also consistent with the congruent dissolution of olivine crystals. Table 9 shows that minor elements are mainly below detection limits in the pristine glass (except for TiO_2 in particle #7.42 and P_2O_5 in #21.65 and #LK06-0050). Mn is present in the pristine glass of #7.42, #21.75 and #LK06-0050, but absent in their alteration products. Na_2O and K_2O are below detection limit in all particles - except in the alteration products of #21.65 and #LK06-0050. Sulphur is observed in the alteration products of #7.42, #21.65 and #LK06-0018. As for V-type cosmic spherules, addition of minor elements foreign to the alteration products (i.e. Na, K and Ti) can be attributed to the weathering of other Na, K and Ti-bearing minerals in the vicinity of the cosmic spherules.

4.1.3. Metal and sulphides

Tables 5 and 6 show the major element compositions of pristine FeNi metal droplets and of their weathering products, respectively. Low totals in the WDS analyses suggest that the alteration phases of metal droplets are hydrous Fe-oxides (i.e., oxyhydroxides). In all cases, the original texture of the metal droplet is conserved, as particularly obvious for particle #LK06-0059 (Fig. 8b), in which the FeNi metal has been almost completely altered, whereas the sulphide is partially preserved. This pattern of alteration is consistent with observations in chondritic meteorites, in which the FeNi metal phases (i.e., kamacite and taenite) are altered into Fe-oxide/oxyhydroxide (i.e., goethite, lepidocrocite and maghemite; Buchwald and Clarke, 1989) and are more susceptible to weathering than sulphides (typically troilite; Bland et al., 2006). In particle #LK06-0074 (Fig. 8f and 8h), the dendritic nature of the magnetite present on the margin of the metal droplet suggests that oxidation of the FeNi metal by atmospheric oxygen during particle formation occurred. It is noteworthy that Fe/Ni ratios in weathering products are higher than that of primary FeNi metal. As metal droplets are the only significant source of Ni in weathering products observed in micrometeorites, the increase of Fe/Ni suggest that a large part of Ni is removed from the micrometeorites in solution. The removal of Ni during weathering may be explained by the circulation of acid water since this element is particularly mobile in low pH aqueous fluid (Smith, 2007).

A sphere of Fe-oxide resulting from the alteration of FeNi metal is also observed in the G-type cosmic spherule #LK06-0027 (Figs. 2o and 3l). Table 7 shows the major elements composition of the Fe-oxide constituting the sphere, the encrustation, and the secondary material filling radial cracks. High Fe and Ni contents suggest that this is the result of weathering of a FeNi metal droplet. The detection of lithophile elements, such as Si, Al and Mg, suggests that the interstitial glass present between the dendrites of magnetite was partially weathered. The presence of detectable amounts of Na, Cl and P, which are usually absent from G-type cosmic spherules, suggests that weathering occurred in an open system.

4.1.4. Magnetite and wüstite

A set of 20 I-type cosmic spherules from the LK collection was investigated to look for evidence of alteration of magnetite and wüstite. Magnetite also forms shells surrounding both scoriaceous and unmelted micrometeorites. I-type cosmic spherules are mainly made of magnetite and wüstite intergrowths (Genge et al., 2008). In all the particles studied here, magnetite grains of all sizes were not altered and preserved their structure and composition, even in areas where other mineral phases are severely weathered (e.g., the preservation of the magnetite rim in the severely weathered coarse-grained, unmelted micrometeorites #19b.24 and #19b.25; Figs. 4c and 4d). By studying the magnetic properties of micrometeorites from the TAM, Suavet et al. (2009) showed that under Antarctica's climatic conditions, magnetite does not alter into maghemite. In addition, magnetite is known to be metastable in the Antarctic environment (Bland et al., 2006).

Below 570°C, wüstite is metastable and can only be preserved in both micrometeorites and the fusion crust of meteorites by quenching (Brownlee, 1981). In most terrestrial environments, wüstite slowly decomposes into magnetite and α-iron. However, in the studied I-type cosmic spherules wüstite has been entirely preserved. This is also the case in I-type cosmic spherules from the TAM collection (Rochette et al., 2008).

The preservation of both magnetite and wüstite in micrometeorites from both the LK and the TAM collections suggests that over their period of storage in the Antarctic environment, these two mineral phases were not altered to an extent observable with the techniques used for this study.

4.2. Weathering products

Weathering products are frequently observed in weathered micrometeorites from both the LK and TAM collections. In particular, the observation of secondary products in dissolved crystals of olivine along a crack running through the CC cosmic spherule #LK06-0091 suggest that cracks are particularly important for the circulation of fluids responsible for the weathering of the particles (Fig. 3b). The composition of the secondary products in CC cosmic spherules #LK06-0044, #18c.01 and #20.02, with significant amounts of S and K associated with high Fe, indicate that a sulphate (likely jarosite) may be present amongst the secondary products of these three particles (Table 3). FTIR spectra of altered areas of particles #20.01 and #20.02 show that sulphate is part of the weathering products (Fig. 6). Jarosite is also present as a weathering product in scoriaceous micrometeorite #6.19 and unmelted micrometeorites #20c.343 and #20c.344 (Table 2).

Jarosite has been described as a weathering product in many micrometeorites from the TAM collection (Rochette et al., 2008). The presence of jarosite in voids suggests that alteration may have mainly occurred due to the circulation of a limited amount of sulphate-rich, acidic water in vesicles over short periods at a time. Assuming that it was emplaced during weathering of the particles, the presence of jarosite is consistent with the congruent nature of the dissolution of olivine crystals which is also associated with acid conditions (Liu, 2006). In particle #6.19, weathering by acidic water can also explain the presence of a euhedral and partially dissolved Si-rich mineral containing minor amounts of Fe, Mg and S, as the preferential removal of M^{2+} cations (i.e. Mg^{2+} and Fe^{2+}) from a relict olivine grain during the first stage of dissolution occurs in acidic fluids (Liu, 2006). Furthermore, Liu (2006) showed that after removal of M^{2+} cations, dissolution of olivine is congruent. This process can also explain the occurrence of Mg-poor areas surrounding remnant pristine olivine in coarse-grained, unmelted micrometeorite #19b.24 (Fig. 4c).

The compositions of altered metal and sulphide droplets, which show notable amounts of Si, S, Al, and Ca, and minor Cl and Mg, are very similar to the composition of “sialic” rust observed in Antarctic meteorites by Gooding (1986a), except for the very high content in S (Table 6). In scoriaceous micrometeorites, the composition of limonite lining the walls of vesicles in #LK06-0095 and #LK06-0096 is very similar to metallic rust and sialic rust, respectively (close-ups of Figs. 5a and 5b). It appears that although these two particles do not appear to have been weathered to a great extent, signs of aqueous weathering are still present. Sialic rust is also observed as secondary material in negative crystals of olivine in coarse-grained unmelted micrometeorite #20c.344 (Fig. 4b; Table 10). Such sialic rust is the result of weathering of mafic silicates from the meteorites (in contrast with the metallic rust, which is the alteration product of FeNi metal in Antarctic meteorites; Gooding, 1986a). Thus, the presence of Si, Al, Ca and minor Mg could be the result of the alteration of mafic minerals in the particles, or the influx of lithophile elements in the solution by aqueous fluids. High abundance in S can be explained by the weathering of the sulphides present in metal droplets. Chlorine present in the alteration product is, however, demonstrably terrestrial, as it is absent from the original micrometeorites in detectable quantities. A likely source for Cl is sea-spray, as suggested from the study on weathering in meteorites (Bland et al., 2006). It is noteworthy that in some cases, olivine crystals adjacent to S-bearing, altered metal droplets appear to have been partially dissolved (e.g., Fig. 8c). This can be explained by the fact that during weathering, part of the S from the sulphides will be added to the alteration fluids as SO_2, which will lower the pH of the solution (Bland and Rolls, 1998), thus facilitating the dissolution of silicates adjacent to the metal droplets.

From SEM observations, it appears that particles #19b.24 and #19b.25 have suffered weathering to a greater extent that #20c.343 and #19b.13 (Fig. 4). Table 10 shows that the composition of the rust encrusting particles #19b.24 and #19b.25 is similar to the metallic rust observed in #19b.13, although with a significant depletion in lithophile elements. The rust filling negative crystals of olivine in #19b.24 has a composition more similar to the sialic rust, whereas the rust in the inner part of #19b.25 has a similar composition to the metallic rust encrusting it. Element maps show that the abundance of Fe-oxide is significantly higher in #19b.24 compared to #19b.25 (Figs. 4c1 and 4d1). Furthermore, olivine seems totally absent from #19b.24, whereas partially dissolved crystals of olivine are still observed in #19b.25. These observations suggest that #19b.24 is weathered to a much greater extent than #19b.25, suggesting that as weathering progresses, Si, Al and P are removed from the system. This is consistent with element mobilization during the weathering of ordinary chondrites in the Antarctic environment (Bland et al., 2006).

4.3. The weathering of fine-grained unmelted micrometeorites

The fine-grained unmelted micrometeorites studied did not show any evidence for weathering down to the micrometer-scale. This class of micrometeorites is mainly associated with CI/CM chondritic material that is rich in phyllosilicates (Genge et al., 2008). Phyllosilicates are rare in these particles though, as they are frequently dehydrated during the atmospheric entry heating to form amorphous dehydroxylates that further decompose into olivine, pyroxene and glass. The reason why we have not observed evidence of weathering in the studied fine-grained unmelted micrometeorites is not clear and might be explained by: (1) the low strength of this material and, thus, its low resistance to physical weathering that will fragment the particles; (2) their stronger resistance to weathering, although their mineralogy and chemistry, especially of the more thermally altered fine-grained unmelted micrometeorites, do not differ greatly from other types of micrometeorites; (3) the rarity of this type of particles results in a small number of particles studied, which as a consequence lowers the probability of finding fine-grained unmelted micrometeorites altered to a significant level.

4.4. The relative weathering of the mineral phases

To understand the process of weathering of micrometeorites, it is important to know the sequence of alteration in terms of the various mineralogical and textural components. As mentioned earlier, olivine will likely be the first component to weather. Within a set of 31 Po cosmic spherules studied, glass appears to be weathering more slowly than olivine in most particles. In order to quantify this, particles can be classified into three groups based on the degree of alteration of olivine crystals and glass: (1) only olivine crystals were altered in 12 particles (or considerably more altered than the glass); (2) glass and olivine were both altered in 17 particles, although weathering seems to have slightly more affected olivine; (3) glass was significantly more weathered than olivine in only 2 particles. Figure 10 shows the ranges of fayalite content of olivine crystals in these three different groups. Figure 11 shows the major element composition of pristine glass in 20 particles. Olivine with a composition of $<Fa_{25}$ was preferentially weathered, whereas olivine with a composition $>Fa_{30}$ was preserved. Olivine crystals with intermediate composition were either weathered or preserved. It is noteworthy that no correlation is found between the major element composition of the glass and its degree of weathering; thus, the weathering of glass appears to be a complex process that is controlled by factors other than its chemical composition (e.g., structure of the glass, temperature, composition of the leachant, etc.; Farges et al., 2007). Studies on the weathering of terrestrial basalts have shown that acidity of the weathering fluid (i.e., water) controls the time persistence of primary minerals such as glass and olivine (e.g., Hausrath et al., 2008). Olivine will weather more rapidly than basaltic glass when the pH ranges between ~2 and ~8. It has been shown that the pH of the snow melt in Antarctica is slightly acidic (Delmas et al., 1982). It is, therefore, reasonable to assume that under the conditions in which the micrometeorites studied here were altered, olivine will tend to be less resistant to weathering than glass.

Undersaturation of with respect to olivine of the surface snow and meltwater in the dry valleys in Antarctica facilitates the congruent dissolution of olivine (Delmas et al., 1982; Green and Canfield, 1984; Green et al., 1988; Green et al., 1989; Wentworth et al., 2005). Based on our observations, Mg-rich olivine appears to be more sensitive to weathering relative to fayalite compositions. This is problematic, as experimental studies and field observations have shown that fayalitic olivine is typically more sensitive to weathering than forsteritic olivine, even under extremely cold conditions (e.g., Westrich et al., 1993; Stopar et al., 2006; Olsen and Rimstidt, 2007; Velbel, 2009; M. A. Velbel, 2014). In contrast, a study by Gislason and Arnórsson (1993), focusing on the weathering of primary basaltic minerals including olivine in cold, silica-undersaturated water from Iceland, observed that increasing forsterite content decreased the stability of olivine.

Based on the observations of preferential weathering of magnesian olivine in cosmic spherules, the sequence of alteration of phases within micrometeorites depends on olivine composition. In those particles with magnesian-rich olivine ($<Fa_{25}$) glass dissolution occurs

after olivine, whilst in those particles with iron-bearing olivine, glass dissolution occurs largely prior to olivine weathering. The sequence of weathering controls the size and shape of cavities generated through dissolution.

Figures 8b and 8g show that the FeNi metal constituting the metal droplets observed in cosmic spherules weather before sulphide. In turn, the generally advanced weathering stage of metal droplets compared to silicate phases suggests that sulphide weathers before olivine and glass. Conversely, magnetite is particularly resistant to weathering in the Antarctic environment and will weather after olivine and glass. Thus, a simple sequence of alteration for cosmic spherules is as follows: FeNi metal<sulphide<olivine<glass<<magnetite (for olivine with $<Fa_{25}$); FeNi metal<sulphide<olivine/glass<<magnetite (for olivine with Fa_{25-30}); FeNi metal<sulphide<glass<olivine<<magnetite (for olivine with $>Fa_{30}$). Scoriaceous micrometeorites have the same overall mineralogy as the cosmic spherules (Genge et al., 2008), so it is reasonable to assume that the alteration sequence of their mineral phases will be the same.

The alteration sequence of mineral phases constituting chondritic coarse-grained unmelted micrometeorites is slightly more complex, as they preserve the chondritic mineralogy of their parent material. In #20c.343 and #19b.13, olivine has been partially dissolved, as indicated by abundant etch pits. Other phases, including pyroxene, oligoclase and glass have been perfectly preserved in both particles. Thus, it appears that olivine is the first silicate mineral to alter. It has been shown that in Antarctic meteorites, olivine and pyroxene are weathered at the same rate (Bland et al., 2006). Thus, it appears that in the case of ordinary chondritic material, micrometeorites from Antarctica present a different weathering sequence than meteorites. The presence of jarosite in voids in #20c.343 and #19b.13 may explain this difference, as the presence of an associated acidic fluid may have considerably accelerated the dissolution of olivine crystals with respect to other silicates. Based on their mineralogy and abundance of secondary phases with respect to primary phases, we suggest that the sequence of weathering of these four coarse-grained unmelted micrometeorites goes as follow: #20c.343 < #19b.13 ≤ #19b.25 < #19b.24. Absence of significant amounts of FeNi metal and sulphide in all particles associated with presence of Ni and S in the weathering products suggests that FeNi metal and sulphide are more susceptible to weathering than olivine, which is, in turn, more susceptible than glass/feldspar and pyroxene. Furthermore, the element map of #19b.24 shows that pyroxene is the mineral phase most resistant to weathering, as it is the only observed silicate phase. We, thus, propose the following sequence of alteration for coarse-grained micrometeorites: FeNi metal/sulphide < olivine < feldspar/glass < pyroxene.

5. Implications

5.1. Rates of weathering of micrometeorites.

Rates of weathering of micrometeorites can be determined using a range of different methods. A simple method would be to compare the residence age of individual micrometeorites on the Earth's surface with their degree of weathering. Rochette et al. (2008) showed that the minimum period of accumulation for micrometeorites in the TAM collection is ~1 Ma based on the presence of Australasian microtektites. Suavet et al. (2011) managed to constrain the residence age of a set of cosmic spherules from the TAM by studying their paleomagnetic properties related to Earth's geomagnetic field polarity. They demonstrated that cosmic spherules older than 0.78 Ma (i.e., older than the last geomagnetic reversal; Bassinot et al., 1994) show a higher degree of weathering (i.e., dissolution of olivine and encrustation with jarosite) than cosmic spherules younger than this age. Although this work indicates that the residence age of cosmic spherules in the TAM collection can be extremely long and, thus, that weathering is particularly slow, the determined age is not absolute and does not allow calculation of the weathering rates of the cosmic spherules.

Micrometeorites from the South Pole Water Well and Concordia collections have better constrained terrestrial residence time, at 1 ka and a few tens of years, respectively (Taylor et al., 1998; Duprat et al., 2007). Their terrestrial age is too short for them to have suffered extensive weathering and precludes determination of weathering rates. A meaningful weathering scale, which accounts for relative alteration susceptibilities and identifies a sequence of weathering effects, although not quantitative can provide constraints by which approximate relative ages could be evaluated.

5.2. A weathering scale for micrometeorites.

A weathering scale for micrometeorites would allow assessment of their survival in the terrestrial environment and would improve the evaluation of the micrometeorite flux to Earth. A weathering scale originally used by the NASA Johnson Space Center for Antarctic meteorites consisted of the three distinct categories A, B and C, which indicate the level of rustiness of a hand specimen. This scale was later improved by Velbel (1988) to indicate by the addition of a lower "e" to the original classification the presence of evaporites formed as a result of terrestrial weathering on Antartic meteorites. The scale was then adapted to thin sections by (Jull et al., 1991) and was based on the progressive replacement of FeNi metal, troilite and then silicates by their weathering products. The scale was then updated by Wlotzka (1993) and is easy to use, as it only requires a survey of a polished thin section of a sample using an optical microscope. A similar weathering scale was developed for CR and CK carbonaceous chondrites (Rubin and Huber, 2005). The response to weathering of different classes of meteorites (e.g., ordinary or carbonaceous chondrites) differs greatly, as their primary mineralogy and chemistry are fundamentally different (Bland et al., 2006). A universal scale of weathering for all types of meteorites may then not be possible. The same limitations apply to micrometeorites, as mineralogy and chemistry vary considerably depending on the various types. Similarly to meteorites, we have shown that micrometeorites of the same subtype (and sometimes the same type) will weather following a precise sequence of alteration (e.g., FeNi metal and sulphide first, followed by silicates and glass). However, it is not possible to extend a unique sequence of alteration to all micrometeorite types due to their disparate mineralogies, compositions and small volumes. For example, glass chemical compositions are fundamentally different in glass and Po cosmic spherules. As large variations in glass composition may affect their rate of weathering, it appears that a unique weathering scale for these two types of micrometeorites may not accurately reflect their relative terrestrial residence age.

Alternatively, we propose a weathering scale applicable to the different micrometeorite types that is not correlated with their terrestrial ages. The proposed bimodal classification is based upon the degree of weathering against the level of encrustation by secondary material. These two criteria were chosen firstly because they often form independently from one another, as the encrustation present on the particles may originate from processes foreign to the micrometeorite (e.g., growth of salts in the LK moraine or TAM micrometeorite traps). Secondly, they are easily identified using optical microscopy on sectioned samples, similarly to the weathering scale for ordinary chondrites (Jull et al., 1991; Wlotzka, 1993). The degree of weathering includes loss of primary minerals (e.g., loss of silicates by congruent dissolution) and replacement of mineral phases (e.g., FeNi metal and glass altered to Fe-oxide/oxyhydroxide and palagonite, respectively). The following stages of weathering are distinguished:

- 0: No visible loss and/or alteration of primary material.
- 1: Minor loss and/or alteration of primary material.
- 2: Moderate loss and/or alteration of primary material (20-60%).
- 3: Severe loss and/or alteration of primary material (>60%).

The level of encrustation surrounding the particles by secondary phases can be divided into three different stages:

- A: No visible encrustation.
- B: Partial encrustation.
- C: Complete encrustation.

A weathering scale is shown in Table 11. Micrometeorites showing neither visible effects of weathering nor encrustation will be classified 0A, whereas micrometeorites showing both severe weathering and complete encrustation will be classified as 3C. Using this weathering scale, the following micrometeorites of this study can be classified as follow: V-type cosmic spherule #LK06-0036 (Fig. 2j) as 1A; BO cosmic spherule #LK06-0038 (Fig. 2e) as 2A; Po cosmic spherule #21.66 (Fig. 2c) as 3A; I-type cosmic spherule #LK06-0027 as 2B (Fig. 2o); and coarse-grained unmelted micrometeorites #19b.25 and #19b.24 (Figs. 4c and 4d) as 3B and 3C, respectively.

This weathering scale may prove useful for quickly and efficiently estimating to which extent various collections of Antarctic micrometeorites are affected by terrestrial weathering. Furthermore, the absence of a proper weathering scale results in the terrestrial weathering being often overlooked when looking for possible biases in micrometeorite collections.

5.3. Effects on preservation and abundance of micrometeorites

The observations made on the relative stability of phases within micrometeorites in the Antarctic environment have implications for the preservation and abundance of particles within accumulation deposits on the continent. A key feature of micrometeorite weathering is the preferential removal of olivine compared with glass, with enhanced dissolution of Mg-rich olivine. Particles in which Mg-rich olivine are a key component, such as Po cosmic spherules and type I coarse-grained unmelted micrometeorites (Genge et al., 2008), are likely to experience increases in pore space and permeability that will further enhance their susceptibility to alteration through the penetration of snow melt. Dissolution is also likely to affect the mechanical strength of particles, with those experiencing significant dissolution perhaps undergoing fragmentation during freeze-thaw events and, thus, a decrease in abundance at larger sizes relative to other particles. Such mechanical effects may be expected to be most significant in moraine deposits and traps on rock surfaces where long term exposure to minor climatic divergences is most likely. Particles trapped in snow or ice being less likely to be influenced by short term changes in temperature.

Dissolution of crystalline phases may also influence accumulation of micrometeorites in those deposits in which secondary accumulation of wind-blown dust occurs. Moraines formed in the lee of nunataks are likely to, in part, act as aeolian traps with enhanced accumulation and retention of denser particles. Removal of olivine by dissolution will cause decreases in particle density that may allow preferential loss of these particles if a deposit is intermittently exposed at the surface by removal of snow cover decreasing the abundance of such particles.

Precipitation of secondary phases within micrometeorites is likely to have a complex effect on their alteration. Within cavities secondary phases will decrease permeability and impede further dissolution of primary phases. Such effects may, in particular, affect particles with etched rims, whose outermost portions can be sealed by precipitation of secondary phases.

Micrometeorites represent a large part of the flux of extraterrestrial matter to Earth's (Borwnlee, 1981), therefore determining these preservation biases with precision can have a significant impact when estimating the nature of this flux and its variability over the recent geological past.

5.4. Environmental factors controlling the weathering of micrometeorites.

Despite the arid and cold conditions in Antarctica, we have shown that indicators of chemical weathering are frequent in Antarctic micrometeorites. The presence of hydrous secondary mineral phases (e.g., Fe-oxyhydroxide, jarosite and palagonite-like gel) and the congruent dissolution of olivine suggest that availability of liquid water is the main factor controlling weathering. Furthermore, the addition of elements foreign to the host micrometeorite in secondary products (e.g., Cl in secondary Fe-oxyhydroxide) suggests that weathering occurs in an open system, with water adding and removing elements from the micrometeorites as weathering progresses. The open system nature of the alteration suggests that water is able to infiltrate and flow into the upper few centimeters of the moraine (in the case of the LK collection) or of the granitic detritus in micrometeorites traps (i.e., regarding the TAM collection) rather than forming as menisci of water attached to a few grains. This implies significant melting of snow and fluid flow. Localised melting of snow in the arid areas of Antarctica is common on solar-heated boulders (Marchant and Head, 2007), but the absence of such large rocks on the sampling site of the LK moraine suggests that the melting of snow was not a localised event - perhaps suggesting climatic variations.

The observation of frequent laminations in palagonite-like gel in V-type cosmic spherules (e.g., Figs. 3h-j) and in encrustations of Fe-oxyhydroxide (e.g., Figs. 3a and 4d) on the margins of micrometeorites suggests that the inflow of liquid water does not occur continuously. This is consistent with seasonal melting of snow present in the micrometeorite traps when the ground temperature in both Northern Victoria Land and the Queen Maud Mountains rises above 0°C (LaPrade, 1986; Prick et al., 2003). We have also observed single V-type cosmic spherules showing different weathering types that are related to different water/rock ratios. This suggests that the seasonal variations of temperature will not produce abundant liquid water uniformly in the moraine, but rather in limited areas, likely at the mm to cm scale.

Jarosite is usually unstable under temperate and tropical climate and decomposes to produce ferric oxyhydroxides, but the lack of continuous input of sufficient quantity of water to the micrometeorite traps may prevent jarosite from decomposing, leaving it metastable under these conditions over long periods of time (Madden et al., 2004). Micrometeorites from the TAM collection have accumulated over the last 1 Ma, and the climatic conditions in Antarctica have been roughly stable over this period of time, suggesting that jarosite formed in a particularly cold and dry environment (Jouzel et al., 2007). Constituents of jarosite in the TAM micrometeorite traps are likely derived from the weathering of granitic material (especially for K) and of micrometeorites (Fe). The presence of SO_4 can result from the weathering of sulphide occasionally present in the micrometeorites. On the other hand, in micrometeorites devoid of sulphide, the source of SO_4 is necessarily external. A possible external source of S in the jarosite of micrometeorites from the TAM are tephra, commonly found in the region (Curzio et al., 2008) and in the micrometeorite traps (Rochette et al., 2008). A close proximity between Northern Victoria Land with the Ross Sea and Pacific

Ocean suggest that sea sprays may be another good source for SO_4 (Delmas et al., 1982; Gibson et al., 1983). Furthermore, sulphates (and in particular jarosite) are present in much lesser quantity in micrometeorites from LK. Even though the extent of the Ross Ice Shelf has been variable over the last 1 Ma (Pollard and DeConto, 2009), it is reasonable to assume that the LK area has been less exposed to sea sprays than the Northern Victoria Land, although the presence of jarosite within LK, combined with the generally antipolar nature of low altitude winds, may necessitate ingress of the ice edge into the Ross Sea over the accumulation lifetime of the LK deposit. This observation strengthens the idea that SO_4 in jarosite might in part come from sea sprays. An important implication for the formation of jarosite is that the water controlling the weathering of micrometeorites is acidic (Swayze et al., 2008). The congruent dissolution of olivine and the presence of etch pits during the first stage of alteration also support weathering in an acidic environment (Velbel, 2009). The preferential dissolution of olivine adjacent to altered sulphide-bearing metal droplets in cosmic spherules suggests that in some cases the increase in acidity of the weathering fluid due to formation of SO_4 may have been very localised (e.g., Fig. 8b and 8c). Finally, jarosite has been observed on the surface of Mars by the Opportunity rover (Christensen et al., 2004; Klingelhöfer et al., 2004). Therefore, another important implication for the presence of jarosite as a weathering product in micrometeorites is that, in addition to the McMurdo Dry Valleys (Wentworth et al., 2005), the glacial moraines and ice-free tops of nunataks of the Transantarctic Mountains may be good analog sites for the surface of Mars.

6. Conclusions

Based on this study of micrometeorites from the Larkman Nunatak (LK) ($n = 366$) and from the Transantarctic Mountains (TAM) collection ($n = 25$), we have shown that the effects of terrestrial weathering frequently obscure the primary features of micrometeorites from Antarctica.

In all types of micrometeorites, we have observed several categories of weathering effects that vary between particle types and between individual particles of the same type. The main weathering effects include the creation of irregular and faceted cavities, etch pits in olivine crystals, infilled cavities, replaced silicate phases, and hydrated and replaced metal. Irregular and faceted cavities and etch pits are the result of the dissolution of olivine crystals. Cavities are then frequently filled with fine-grained polycrystalline secondary products mainly composed of Fe-oxide/oxyhydroxide. The replaced silicate phases consist predominantly of altered glass in the form of a palagonite-like gel. Fe-Ni metal and sulphide are rapidly altered to Fe-oxide/oxyhydroxide.

Micrometeorites generally consist of several minerals and as a consequence are affected by differential weathering. By studying micrometeorites exhibiting different degrees of weathering, we have been able to determine a sequence of alteration of their various mineral phases. The sequence of alteration for cosmic spherules and scoriaceous micrometeorites is as follows: FeNi metal<sulphide<olivine<glass<<magnetite (for olivine with $<Fa_{25}$). Coarse-grained unmelted micrometeorites generally have a slightly more complex mineralogy than cosmic spherules and scoriaceous micrometeorites. The sequence of alteration of their mineral phases is: FeNi metal/sulphide < olivine < feldspar/glass < pyroxene.

Determining absolute weathering rates of micrometeorites from the LK and TAM collection was not possible. In order to do so, future work may consist in the development of techniques that allow constraining the absolute age of individual particles exhibiting various degrees of weathering. Despite the high variability in mineralogy and chemistry between the different groups of micrometeorites, we propose a weathering scale for micrometeorites based on both the degree of weathering (i.e., loss and/or alteration of primary material) and the level of encrustation by secondary phases. These two criteria are not interdependent and are easily observable. The following stages of weathering are distinguished:

- 0: No visible loss and/or alteration of primary material.
- 1: Minor loss and/or alteration of primary material (mainly silicate phases).
- 2: Moderate loss and/or alteration of primary material (20-60%).
- 3: Severe loss and/or alteration of primary material (>60%).

These stages are then combined with the level of encrustation surrounding the particles, which is divided into three different stages:

- A: No visible encrustation.
- B: Partial encrustation.
- C: Complete encrustation.

Finally, environmental factors controlling the weathering of micrometeorites have been determined:

- Mineralogical and textural evidence indicates that water is the main agent controlling the weathering of micrometeorites.

- The observation of etch pits in olivine shows that the weathering occurred in an abiotic environment.

- The presence of jarosite and the congruent dissolution of olivine show that the water controlling the weathering of micrometeorites was acidic.

- The chemistry of secondary mineral phases shows that weathering occurs in an open system, which, in turn, shows that occasional melting of snow produced liquid water in the first few centimeters of the LK moraine and in the micrometeorites traps of the TAM.

- The observation of laminations in palagonite and of several types of weathering related to different water/rock ratios in individual V-type cosmic spherules shows that melting of snow resulting from seasonal variations is not uniform on the moraine but rather will affect limited areas in a distinct manner.

Acknowledgments

This work was supported by the Science and Technology Facilities Council (STFC) [grant number: ST/J001260/1]. A. Kearsley, A. Ball and T. Goral (NHM London) are thanked for assistance during analytical sessions. LF is supported by the Italian *Programma Nazionale delle Ricerche in Antartide* (PNRA) through the PEA2013 AZ2.04 "Meteoriti Antartiche" project, and by Pisa University's *Fondi di Ateneo.* We also like to acknowledge the contributions of four reviewers, Prof Micheal A. Velbel, Prof Martin Lee, Prof Pierre Rochette and Dr Ashley King, for their helpful suggestions.

References:

Bassinot F. C., Labeyrie L. D., Vincent E., Quidelleur X., Shackleton N. J. and Lancelot Y. (1994) The astronomical theory of climate and the age of the Brunhes-Matuyama magnetic reversal. *Earth Planet. Sci. Lett.* **126**, 91–108.

Bishop J. L. and Murad E. (2005) The visible and infrared spectral properties of jarosite and alunite. *Am. Mineral.* **90**, 1100–1107.

Blackhurst R. L., Genge M. J. and Grady M. M. (2004) Microbial D/H Fractionation in Extraterrestrial Materials: Application to Micrometeorites and Mars. *Abstr. Lunar Planet. Sci. Conf.* **35,** 1584.

Blanchard M., Brownlee D., Bunch T., Hodge P. and Kyte F. (1980) Meteoroid ablation spheres from deep-sea sediments. *Earth Planet. Sci. Lett.* **46**, 178–190.

Bland P. A., Zolensky M. E., Benedix G. K. and Sephton M. A. (2006) Weathering of Chondritic Meteorites. *Meteorites Early Sol. Syst. II*.

Bland W. and Rolls D. (1998) Weathering: an introduction to the scientific principles. Ed. Arnold, London, 271 pp.

Brownlee D. E. (1981) Extraterrestrial components. In *The Sea 7, ed Emiliani C (Wiley, New York)* pp. 733–762.

Brownlee D. E., Bates B. and Schramm L. (1997) The elemental composition of stony cosmic spherules. *Meteorit. Planet. Sci.* **32**, 157–175.

Buchwald V. F. and Clarke R. S. . J. (1989) Corrosion of Fe-Ni alloys by Cl-containing akaganéite (beta-FeOOH): The Antarctic meteorite case. *Am. Mineral.* **74**, 656–667.

Burns R. G. (1993) Rates and mechanisms of chemical weathering of ferromagnesian silicate minerals on Mars. *Geochim. Cosmochim. Acta* **57**, 4555–4574.

Christensen P. R., Wyatt M. B., Glotch T. D., Rogers A. D., Anwar S., Arvidson R. E., Bandfield J. L., Blaney D. L., Budney C., Calvin W. M., Fallacaro A., Fergason R. L., Gorelick N., Graff T. G., Hamilton V. E., Hayes A. G., Johnson J. R., Knudson A. T., McSween Jr. H. Y., Mehall G. L., Mehall L. K., Moersch J. E., Morris R. V., Smith M. D., Squyres S. W., Ruff S. W., Wolff M. J. (2004) Mineralogy at Meridiani Planum from the Mini-TES Experiment on the Opportunity Rover. *Sience* **306**, 1733–1739.

Cordier C., Folco L., Suavet C., Sonzogni C. and Rochette P. (2011) Major, trace element and oxygen isotope study of glass cosmic spherules of chondritic composition: The record of their source material and atmospheric entry heating. *Geochim. Cosmochim. Acta* **75**, 5203–5218.

Crovisier J.-L., Honnorez J., Fritz B. and Petit J.-C. (1992) Dissolution of subglacial volcanic glasses from Iceland: laboratory study and modelling. *Appl. Geochemistry* **7**, 55–81.

Delmas R., Briat M. and Legrand M. (1982) Chemistry of south polar snow. *J. Geophys. Res.* **87**, 4314-4318.

Delvigne J., Bisdom E. B. A., Sleeman J. and Stoops G. (1979) Olivines, Their Pseudomorphs and Secondary Products. *Pedologie* **23**, 247–309.

Duprat J., Engrand C., Maurette M., Kurat G., Gounelle M. and Hammer C. (2007) Micrometeorites from Central Antarctic snow: The CONCORDIA collection. *Adv. Sp. Res.* **39**, 605–611.

Engrand C., Maurette M., Kurat G., Brandstatter F. and Perreau M. (1993) A new carbon-rich phase (COPS) in Antarctic micrometeorites. *24th Lunar Planet. Sci. Conf.*, 441–442.

Farges F., Etcheverry M.-P., Haddi A., Trocellier P., Curti E. and Brown G. E. (2007) Durability of Silicate Glasses: An Historical Approach. In *AIP Conference Proceedings* AIP. pp. 44–50.

Fisk M. R., Popa R., Mason O. U., Storrie-Lombardi M. C. and Vicenzi E. P. (2006) Iron-magnesium silicate bioweathering on Earth (and Mars?). *Astrobiology* **6**, 48–68.

Folco L., D'Orazio M., Tiepolo M., Tonarini S., Ottolini L., Perchiazzi N., Rochette P. and Glass B. P. (2009) Transantarctic Mountain microtektites: Geochemical affinity with Australasian microtektites. *Geochim. Cosmochim. Acta* **73**, 3694–3722.

Folco L., Rochette P., Perchiazzi N., D'Orazio M., Laurenzi M. A. and Tiepolo M. (2008) Microtektites from Victoria Land Transantarctic Mountains. *Geology* **36**, 291.

Furnes H. (1978) Element mobility during palagonitization of a subglacial hyaloclastite in Iceland. *Chem. Geol.* **22**, 249–264.

Genge M. J. (2006) Igneous rims on micrometeorites. *Geochim. Cosmochim. Acta* **70**, 2603–2621.

Genge M. J. (2007) Micrometeorites and Their Implications for Meteors. *Earth. Moon. Planets* **102**, 525–535.

Genge M. J., Engrand C., Gounelle M. and Taylor S. (2008) The classification of micrometeorites. *Meteorit. Planet. Sci.* **43**, 497–515.

Genge M. J. and Grady M. M. (1998) Melted micrometeorites from Antarctic ice with evidence for the separation of immiscible Fe-Ni-S liquids during entry heating. *Meteorit. Planet. Sci.* **33**, 425–434.

Gibson E. K., Wentworth S. J. and McKay D. S. (1983) Chemical weathering and diagenesis of a cold desert soil from Wright Valley, Antarctica: An analog of Martian weathering processes. *J. Geophys. Res.* **88**, A912.

Gislason S. R. and Arnórsson S. (1993) Dissolution of primary basaltic minerals in natural waters: saturation state and kinetics. *Chem. Geol.* **105**, 117–135.

Gooding J. L. (1986a) Weathering of stony meteorites in Antarctica. *Lunar Planet. Inst. Int. Work. Antarct. Meteorites,* 48-54.

Gooding J. L. (1986b) Clay-mineraloid weathering products in Antarctic meteorites. *Geochim. Cosmochim. Acta* **50**, 2215–2223.

Gooding J. L. (1982) Mineralogical aspects of terrestrial weathering effects in chondrites from Allan Hills, Antarctica. *12th Lunar Planet. Sci. Conf.*, 1105-1122.

Grant J. A. (2005) Isocon analysis: A brief review of the method and applications. *Phys. Chem. Earth, Parts A/B/C* **30**, 997–1004.

Grant J. A. (1986) The isocon diagram; a simple solution to Gresens' equation for metasomatic alteration. *Econ. Geol.* **81**, 1976–1982.

Green W. J., Angle M. P. and Chave K. E. (1988) The geochemistry of antarctic streams and their role in the evolution of four lakes of the McMurdo dry valleys. *Geochim. Cosmochim. Acta* **52**, 1265–1274.

Green W. J. and Canfield D. E. (1984) Geochemistry of the Onyx River (Wright Valley, Antarctica) and its role in the chemical evolution of Lake Vanda. *Geochim. Cosmochim. Acta* **48**, 2457–2467.

Green W. J., Gardner T. J., Ferdelman T. G., Angle M. P., Varner L. C. and Nixon P. (1989) Geochemical processes in the Lake Fryxell Basin (Victoria Land, Antarctica). *Hydrobiologia* **172**, 129–148.

Hausrath E. M., Navarre-Sitchler a K., Sak P. B., Steefel C. and Brantley S. L. (2008) Basalt weathering rates on Earth and the duration of liquid water on the plains of Gusev Crater. *Geology* **36**, 67–70.

Jouzel J., Masson-Delmotte V., Cattani O., Dreyfus G., Falourd S., Hoffmann G., Minster B., Nouet J., Barnola J. M., Chappellaz J., Fischer H., Gallet J. C., Johnsen S., Leuenberger M., Loulergue L., Luethi D., Oerter H., Parrenin F., Raisbeck G., Raynaud D., Schilt A., Schwander J., Selmo E., Souchez R., Spahni R., Stauffer B., Steffensen J. P., Stenni B., Stocker T. F., Tison J. L., Werner M. and Wolff E. W. (2007) Orbital and millennial Antarctic climate variability over the past 800,000 years. *Science* **317**, 793–796.

Jull A. J. T., Wlotzka F. and Donahue D. J. (1991) Terrestrial Ages and Petrologic Description of Roosevelt County Meteorites. *Abstr. Lunar Planet. Sci. Conf.* **22**, 667-668.

Jull A. J., Cheng S., Gooding J. L. and Velbel M. A. (1988) Rapid growth of magnesium-carbonate weathering products in a stony meteorite from antarctica. *Science* **242**, 417–9.

Klingelhöfer G., Morris R. V., Bernhardt B., Schröder C., Rodionov D. S., de Souza Jr. P. A., Yen A., Gellert R., Evlanov E. N., Zubkov B., Foh J., Bonnes U., Kankeleit E., Gütlich P., Ming D. W., Renz F., Wdowiak T., Squyres S. W., Arvidson R. E. (2004) Jarosite and Hematite at Meridiani Planum from Opportunity's Mössbauer Spectrometer. *Science* **306**, 1740–1745.

LaPrade K. (1986) Climate, geomorphology, and glaciology of the Shackleton glacier area, Queen Maud Mountains, Transantarctic Mountains, Antarctica eds. M. D. Turner and J. E. Splettstoesser. *Antarct. Res. Ser.* **36**, 163–196.

Lee M. R., Tomkinson T., Mark D. F., Stuart F. M. and Smith C. L. (2013) Evidence for silicate dissolution on Mars from the Nakhla meteorite. *Meteorit. Planet. Sci.* **48**, 224–240.

Liu Y. (2006) Mechanism for the dissolution of olivine series minerals in acidic solutions. *Am. Mineral.* **91**, 455–458.

Losiak A. and Velbel M. A. (2011) Evaporite formation during weathering of Antarctic meteorites--A weathering census analysis based on the ANSMET database. *Meteorit. Planet. Sci.* **46**, 443–458.

Madden M. E., Bodnar R. J. and Rimstidt J. D. (2004) Jarosite as an indicator of water-limited chemical weathering on Mars. *Nature* **431**, 821–823.

Marchant D. R. and Head J. W. (2007) Antarctic dry valleys: Microclimate zonation, variable geomorphic processes, and implications for assessing climate change on Mars. *Icarus* **192**, 187–222.

Maurette M., Jehanno C., Robin E. and Hammer C. (1987) Characteristics and mass distribution of extraterrestrial dust from the Greenland ice cap. **328**, 699–702.

Maurette M., Olinger C., Michel-Levy M. C., Kurat G., Pourchet M., Brandstätter F. and Bourot-Denise M. (1991) A collection of diverse micrometeorites recovered from 100 tonnes of Antarctic blue ice. *Nature* **351**, 44–47.

Morlok A., Bowey J., Kohler M. and Grady M. M. (2006) FTIR 2-16 micron spectroscopy of micron-sized olivines from primitive meteorites. *Meteorit. Planet. Sci.* **41**, 773–784.

Morlok A., Köhler M., Bowey J. E. and Grady M. M. (2006) FT–IR microspectroscopy of extraterrestrial dust grains: Comparison of measurement techniques. *Planet. Space Sci.* **54**, 599–611.

Nesbitt H. W. and Wilson R. E. (1992) Recent chemical weathering of basalts. *Am. J. Sci.* **292**, 740–777.

Olsen A. A. and Rimstidt J. D. (2007) Using a mineral lifetime diagram to evaluate the persistence of olivine on Mars. *Am. Mineral.* **92**, 598–602.

Pollard D. and DeConto R. M. (2009) Modelling West Antarctic ice sheet growth and collapse through the past five million years. *Nature* **458**, 329–32.

Prick A., Guglielmi M. and Strini A. (2003) Rock Weathering in Central Spitsbergen and in Northern Victoria Land (Antarctica). *Marie Curie Fellowsh. Assoc. Ann. III*, 50–55.

Rochette P., Folco L., Suavet C., van Ginneken M., Gattacceca J., Perchiazzi N., Braucher R. and Harvey R. P. (2008) Micrometeorites from the transantarctic mountains. *Proc. Natl. Acad. Sci. U. S. A.* **105**, 18206–18211.

Rubin A. E. and Grossman J. N. (2010) Meteorite and meteoroid: new comprehensive definitions. *Meteorit. Planet. Sci.* **45**, 114-122.

Rubin A. E. and Huber H. (2005) A weathering index for CK and R chondrites. *Meteorit. Planet. Sci.* **40**, 1123–1130.

Rudraswami N. G., Prasad M. S., Plane J. M. C., Berg T., Feng W. and Balgar S. (2014) Refractory metal nuggets in different types of cosmic spherules. *Geochim. Cosmochim. Acta* **131**, 247–266.

Sanders D. M. and Hench L. L. (1973) Mechanisms of Glass Corrosion. *J. Am. Ceram. Soc.* **56**, 373–377.

Smith K. S. (2007) Addressing the toxic legacy of abandoned mines on public land in the western United States, in Understanding and Responding to Hazardous Substances at Mine Sites in the Western United States, R*ev. Eng. Geol.* **17**, 25-47.

Staudigel H. and Hart S. R. (1983) Alteration of basaltic glass: Mechanisms and significance for the oceanic crust-seawater budget. *Geochim. Cosmochim. Acta* **47**, 337–350.

Stefánsson A., Gíslason S. R. and Arnórsson S. (2001) Dissolution of primary minerals in natural waters. *Chem. Geol.* **172**, 251–276.

Sterpenich J. and Libourel G. (2001) Using stained glass windows to understand the durability of toxic waste matrices. *Chem. Geol.* **174**, 181–193.

Stopar J. D., Jeffrey Taylor G., Hamilton V. E. and Browning L. (2006) Kinetic model of olivine dissolution and extent of aqueous alteration on mars. *Geochim. Cosmochim. Acta* **70**, 6136–6152.

Stroncik N. A. and Schmincke H.-U. (2002) Palagonite – a review. *Int. J. Earth Sci.* **91**, 680–697.

Suavet C., Gattacceca J., Rochette P. and Folco L. (2011) Constraining the terrestrial age of micrometeorites using their record of the Earth's magnetic field polarity. *Geology* **39**, 123–126.

Suavet C., Gattacceca J., Rochette P., Perchiazzi N., Folco L., Duprat J. and Harvey R. P. (2009) Magnetic properties of micrometeorites. *J. Geophys. Res.* **114**, B04102.

Suavet C., Rochette P., Kars M., Gattacceca J., Folco L. and Harvey R. P. (2009) Statistical properties of the Transantarctic Mountains (TAM) micrometeorite collection. *Polar Sci.* **3**, 100–109.

Swayze G. A., Desborough G. A., Smith K. S., Lowers H. A., Hammarstrom J. M., Diehl S. F., Leinz R. W. and Driscoll R. L. (2008) Understanding Jarosite—From Mine Waste to Mars. *U.S. Geol. Surv. Circ.* **1328**, 8–13.

Taylor S., Lever J. H. and Harvey R. P. (1998) Accretion rate of cosmic spherules measured at the South Pole. *Nature* **392**, 899–903.

Taylor S., Matrajt G. and Guan Y. (2012) Fine-grained precursors dominate the micrometeorite flux. *Meteorit. Planet. Sci.* **47**, 550–564.

Terada K., Yada T., Kojima H., Noguchi T., Nakamura T., Murakami T., Yano H., Nozaki W., Nakamuta Y., Matsumoto N., Kamata J., Mori T., Nakai I., Sasaki M., Itabashi M., Setoyanagi T., Nagao K., Osawa T., Hiyagon H., Mizutani S., Fukuoka T., Nogami K., Ohmori R. and Ohashi H. (2001) General characterization of Antarctic micrometeorites collected by the 39th Japanese Antarctic Research Expedition: Consortium studies of JARE AMMs (III). *Antarct. Meteor. Res.* **14**, 89–107.

Van Ginneken M., Folco L., Cordier C. and Rochette P. (2012) Chondritic micrometeorites from the Transantarctic Mountains. *Meteorit. Planet. Sci.* **47**, 228–247.

Van Ginneken M., Folco L., Perchiazzi N., Rochette P. and Bland P. A. (2010) Meteoritic ablation debris from the Transantarctic Mountains: Evidence for a Tunguska-like impact over Antarctica ca. 480ka ago. *Earth Planet. Sci. Lett.* **293**, 104–113.

Velbel M. A. and Gooding J. L. (1990) Terrestrial weathering of Antarctic stony meteorites - developments 1985 - 1989. *Lun. Planet. Inst. Tech. Rep.* **90-01**, 94-98.

Velbel M. A. (2009) Dissolution of olivine during natural weathering. *Geochim. Cosmochim. Acta* **73**, 6098–6113.

Velbel M. A. (2014a) Etch-pit size, dissolution rate, and time in the experimental dissolution of olivine: Implications for estimating olivine lifetime at the surface of Mars. *Am. Mineral.* **99**, 2227–2233.

Velbel M. A. (2014b) Terrestrial weathering of ordinary chondrites in nature and continuing during laboratory storage and processing: Review and implications for Hayabusa sample integrity. *Meteorit. Planet. Sci.* **49**, 154–171.

Velbel M. A. (1988) The Distribution and Significance of Evaporitic Weathering Products on Antarctic Meteorites. *Meteoritics* **23**, 151–159.

Velbel M. A., Long D. T. and Gooding J. L. (1991) Terrestrial weathering of Antarctic stone meteorites: Formation of Mg-carbonates on ordinary chondrites. *Geochim. Cosmochim. Acta* **55**, 67–76.

Wentworth S. J., Gibson E. K., Velbel M. A. and McKay D. S. (2005) Antarctic Dry Valleys and indigenous weathering in Mars meteorites: Implications for water and life on Mars. *Icarus* **174**, 383–395.

Westrich H. R., Cygan R. T., Casey W. H., Zemitis C. and Arnold G. W. (1993) The dissolution kinetics of mixed-cation orthosilicate minerals. *Am. J. Sci.* **293**, 869–893.

Wlotzka F. (1993) A Weathering Scale for the Ordinary Chondrites. *Meteoritics* **28**, 460–460.

Figure captions:

Fig.1. a) Sketch map of Antarctica showing the locations of the Larkman Nunatak (LK), Miller Butte (MB), and Pian delle Tectiti (PT). b) Panoramic view of LK. Arrowed is the sampling area where glacial moraine was collected. c) Detail of the sampling area. Note the 4 cm thick layer of snow on top of the moraine.

Fig. 2. Scanning electron microscope backscattered electrons images of weathered cosmic spherules. a) Po cosmic spherule #LK06-0026 in which olivine crystals nearest to the surface have been removed. b) and c) Po cosmic spherules #7.42 and #21.66 showing high degrees of weathering, with olivine crystals totally dissolved. d-f) BO cosmic spherules #LK06-0038, #LK06-0022 and #LK06-0047 showing various degrees of olivine dissolution. g), h) and i) CC cosmic spherules #LK06-0023, #LK06-0091 and #20.02, showing various degrees of olivine dissolution. j) V-type cosmic spherule #LK06-0036 exhibiting scattered corrosion pits on its surface. k) V-type cosmic spherule #LK06-0119 exhibiting a lamellar discontinuous leached layer. l) V-type cosmic spherule #LK06-0116 exhibiting a continuous leached layer of constant thickness

completely surrounding the particle. m) Magnetite-rich BO cosmic spherule #LK06-0526 showing a high degree of weathering with most olivine crystals having been dissolved. n) An I-type cosmic spherule showing a pristine FeNi metal sphere enclosed in the magnetite and wüstite intergrowth. o) G-type cosmic spherule #LK06-0027 showing pristine magnetite dendrites enclosing an altered FeNi metal sphere. The scale bars are 50 µm. Abbreviations: Ol = olivine; Gl = glass; Pal = palagonite-like gel; Mag = magnetite; Met = FeNi metal; Cav = cavity; FeOx = Fe-oxide; Enc = encrustation.

Fig.3. Scanning electron microscope backscattered electrons images of details of weathering features in cosmic spherules. a) and b) Dissolution features of olivine crystals in CC cosmic spherules. The arrow in (b) indicates a crack along which weathering has progressed. c) Dissolution features in olivine crystals of Po CSs. d) and e) Areas where olivine has been dissolved in BO cosmic spherules. Note that in (e) jarosite has partially replaced dissolved olivine crystals. f) Details of wedge and diamond-shaped etch pits in a Po cosmic spherule. g) Jarosite crystals encrusting a vesicle in BO cosmic spherule #LK06-0526. h) An isolated corrosion pit in a V-type cosmic spherule. i) Discontinuous laminated layer in a V-type cosmic spherule. j) Continuous leached layer in a V-type cosmic spherule. k) Dissolution features in olivine crystals in a coarse-grained cosmic spherule. l) Close-up of an altered FeNi metal in G-type cosmic spherule #LK06-0027 that is enclosed in magnetite. The scale bars are 20 µm. Abbreviations: Ol = olivine; Gl = glass; Pal = palagonite-like gel; Mag = magnetite; Met = FeNi metal; Cav = cavity.

Fig.4. Scanning electron microscope backscattered electrons images of moderately weathered coarse-grained unmelted micrometeorites from the TAM collection. a) Olivine in particle #20c.343 is partially etched out. b) Particle #19b.13 is surrounded by an igneous rim (Genge, 2006). Olivine crystals in both the igneous rim and interior of the particle have

been partially etched out. c) Particle #19b.24, in which primary minerals have been mostly replaced by rust composed of Fe-oxide/oxyhydroxide. d) Particle #19b.25 also shows Fe-oxide/oxyhydroxide rust in negative crystals of olivine. Olivine is partially preserved in the particle. a1, b1, c1, d1 are chemical maps showing the variation in Fe, Mg, Si, Al and Ca contents; and a2, b2, c2 and d2 are chemical maps showing the variation in Fe, K and S contents. The scale bars are 100 µm. Abbreviations: Ol = olivine; Px = Low-Ca pyroxene; Pl = plagioclase; Gl = glass; Mag = magnetite; FeOx = Fe-oxide/oxyhydroxide.

Fig.5. Scanning electron microscope backscattered electrons images of weathered scoriaceous micrometeorites. A-B) particles #LK06-0085 and #LK06-0074, showing linings of secondary material along the border of vesicles. C) Particle #20c.344. Arrows in the close-up indicate cavities filled with jarosite. D) Particle #6.19 is a scoriaceous/coarse-grained micrometeorite, containing >50 vol. %. of relict olivine crystals. Abbreviations: Ol = olivine; FeOx = Fe-oxide/oxyhydroxide; Jar = jarosite.

Fig.6. Mid-infrared reflectance spectra on 50x50 µm areas of cosmic spherule s #20.01 (a), #LK06-0091 (b) and #20.02 (c). Spectra 1, 3 and 5 were acquired on pristine areas and spectra 2, 4, 6 and 7 on altered areas. Spectra on pristine areas are typical of olivine (Morlok et al., 2006). Spectra 4, 6 and 7 of altered areas show bands at ~9.10 µm and ~10.00 µm that can be attributed to sulphate (Bishop and Murad, 2005).

Fig.7. Mid-infrared reflectance spectra on 50x50 µm areas of V-type cosmic spherule s #21p.1 (a) and #7.40 (b). Spectra were acquired over pristine glass (a1-2 and b1) and altered glass (a3-4 and b2-3). In the spectra b2 and b3 sharp band is observed at ~10 µm (dashed line), which can be attributed to sulphate (Bishop and Murad, 2005).

Fig.8. Scanning electron microscope backscattered electrons images of weathered metal droplets in cosmic spherules; a and c) CC cosmic spherule #LK06-0076. b and d) CC cosmic spherule LK06-0059, e and g) Po cosmic spherule #LK06-0085, and f and h) V-type cosmic spherule #LK06-0074. The FeNi metal and sulphide (bright areas) have been partially replaced with Fe-oxide/oxyhydroxide (lighter gray areas). (h) Magnetite dendrites due to the oxidation of FeNi metal during atmospheric entry are visible in particle #LK06-0074.

Fig. 9. Isocon diagrams showing the behaviour of various elements during alteration of the glass in V-type cosmic spherules (Grant, 1986; Grant, 2005). The line CV represents the isocon if the alteration process is assumed to be isovolumetric. The line CM, for constant mass during alteration, is shown for comparison.

Fig.10. Histogram showing 31 Po cosmic spherules from LK grouped according to their fayalite content and the relative degree of alteration of olivine crystals and interstitial glass. “Only glass” means that the glass has been affected by weathering, whereas olivine crystals are intact. “Only olivine” means the opposite situation, whereby only olivine crystals have been affected by alteration. “Olivine + glass” means that both olivine and glass have been affected by alteration to various extents.

Fig.11. Chemical composition of pristine interstitial glasses in Po cosmic spherules from LK (data in wt%).

Table 1. List of micrometeorites studied, classified after Genge et al. (2008)

Types	Larkman[a]	TAM[b]
Cosmic Spherules (CSs)	366	25
Stony	338	25
Porphyritic Olivine (PO)	114	6
Barred Olivine (BO)	109	5
Cryptocrystalline (CC)	38	8
Coarse-grained (CgCS)	16	-
Glass (V)	61	6
Iron (I)	21	-
G-type	7	-
Scoriaceous (ScMM)	-	2
Unmelted (UMM)	-	3
Fine-grained (FgMM)	-	-
Coarse-grained (CgMM)	-	3

[a]Larkman Nunatak collection; [b]Transantarctic Mountains collection.

Table 2. Representative WDS analsyses (in wt.%) of jarosite in micrometeorites from the TAM.

Particle	Al_2O_3	SO_3	K_2O	Fe_2O_3	Total
LK06-0526	0.92	31.1	7.68	41.8	81.5
20.01	0.93	33.4	6.96	38.3	79.6
7.40	1.78	30.5	7.43	37.9	77.6
20c.343	1.06	32.0	7.55	39.3	80.0
20c.344	2.34	32.8	8.26	40.5	83.9

Table 3. Major element compositions (oxide wt%) of secondary products filling negative crystals of olivine in 3 CC and 1 BO cosmic spherules.

Sample	Locality[a]	Target	n		Na_2O	MgO	Al_2O_3	SiO_2	SO_3	K_2O	CaO	Cr_2O_3	MnO	Fe_2O_3	NiO	Total
LK06-0091	LK	Secondary filling	3	avg.	b.d.l.	5.13	6.01	37.2	2.70	b.d.l.	5.55	1.01	b.d.l.	31.2	b.d.l.	88.8
				S.D.		2.38	0.49	1.9	1.80		0.75	0.11		3.1		
LK06-0044	LK	Secondary filling	3	avg.	0.53	0.72	5.98	23.3	22.2	5.59	1.12	b.d.l.	b.d.l.	29.6	b.d.l.	89.0
				S.D.	0.07	0.17	0.11	3.7	0.9	0.37	0.11			2.2		
20.02	MB	Secondary filling	4	avg.	b.d.l.	0.9	6.53	29.2	18.2	4.86	1.23	0.39	b.d.l.	24.0	b.d.l.	85.3
				S.D.		0.16	0.59	5.9	1.3	0.47	0.16	0.30		3.0		
18c.01	MB	Secondary filling	2	avg.	b.dl.	0.50	6.46	14.8	26.8	7.11	0.63	b.d.l.	b.d.l.	27.7	b.d.l.	84.0
				S.D.		0.12	0.77	6.4	2.4	0.72	0.89			2.0		

avg, = averages.

S.D. = Standard deviation.

b.d.l. = below detection limit.

n = number of analyses.

[a] LK = Larkman Nunatak; MB = Miller Butte.

Table 4. WDS analyses of pristine and altered glass cosmic spherules (in oxide wt%).

Particle	Locality[a]	ToW[b]		Na_2O	MgO	Al_2O_3	SiO_2	SO_3	K_2O	CaO	TiO_2	FeO	Total
LK06-0098	LK	CL	avg. pristine	b.d.l.	31.9	2.10	46.5	b.d.l.	b.d.l.	1.28	b.d.l.	17.4	99.5
			S.D. pristine		0.2	0.13	0.7			0.03		0.1	0.7
			avg. altered	0.99	2.68	3.22	47.0	b.d.l.	0.16	1.37	b.d.l.	21.4	77.2
			S.D. altered	0.73	1.27	0.53	2.1		0.20	0.14		1.0	3.6
LK06-0063	LK	CP	avg. pristine	b.d.l.	38.6	2.31	53.9	b.d.l.	b.d.l.	2.25	b.d.l.	4.52	101.7
			S.D. pristine		0.2	0.03	0.1			0.05		0.13	0.2
			avg. altered	0.59	2.98	3.69	52.0	b.d.l.	0.37	1.77	b.d.l.	7.24	68.8
			S.D. altered	0.12	2.18	0.37	3.3		0.29	0.11		0.55	5.0
LK06-0066	LK	CL	pristine	b.d.l.	32.6	1.34	50.2	b.d.l.	b.d.l.	1.36	b.d.l.	14.0	100.5
			avg. altered	0.20	1.92	2.61	48.9	b.d.l.	0.28	2.28	b.d.l.	22.2	79.9
			S.D. altered	0.23	0.23	0.30	3.1		0.21	0.29		2.3	5.5
LK06-0099	LK	CL	avg. pristine	b.d.l.	26.7	2.03	52.2	b.d.l.	b.d.l.	9.70	b.d.l.	10.2	100.9
			S.D. pristine		0.0	0.04	0.4			0.17		0.1	0.3
			avg. altered	0.92	1.90	3.72	51.8	b.d.l.	0.17	2.31	0.47	17.4	79.2
			S.D. altered	0.39	0.13	0.28	0.9		0.30	0.03	0.07	0.5	1.6
LK06-0100	LK	CL	avg. pristine	b.d.l.	30.9	2.12	45.9	b.d.l.	b.d.l.	2.82	b.d.l.	17.2	99.4
			S.D. pristine		0.1	0.08	0.0			0.07		0.2	0.4
			avg. altered	b.d.l.	1.66	4.44	46.5	b.d.l.	0.62	2.21	0.10	26.4	81.9
			S.D. altered		0.13	0.20	1.0		0.14	0.08	0.17	0.4	0.6
LK06-0075	LK	CL + CP	avg. pristine	b.d.l.	31.7	2.76	45.9	b.d.l.	b.d.l.	2.10	b.d.l.	16.5	98.9
			S.D. pristine		0.4	0.11	0.6			0.02		0.2	1.2
			avg. altered	0.43	1.21	4.79	51.1	b.d.l.	0.56	1.18	b.d.l.	14.9	74.2
			S.D. altered	0.09	0.40	0.53	4.5		0.30	0.26		5.2	8.3
LK06-0101	LK	CL	avg. pristine	b.d.l.	30.1	3.17	48.9	b.d.l.	b.d.l.	1.54	b.d.l.	15.7	99.7
			S.D. pristine		0.5	0.16	0.1			0.04		0.1	0.1
			avg. altered	0.47	1.67	5.73	53.6	b.d.l.	1.00	1.84	b.d.l.	17.5	82.9
			S.D. altered	0.04	0.21	0.20	1.1		0.34	0.03		1.4	0.7
LK06-0102	LK	CL	avg. pristine	b.d.l.	28.0	1.58	52.4	b.d.l.	b.d.l.	3.68	b.d.l.	13.3	99.5
			S.D. pristine		0.1	0.04	0.6			0.04		0.3	0.6
			avg. altered	0.37	1.85	2.39	41.9	b.d.l.	0.04	1.69	0.07	15.7	64.2
			S.D. altered	0.22	0.67	0.20	4.2		0.10	0.19	0.15	1.1	5.4

LK06-0103	LK	CL	avg. pristine	b.d.l.	35.7	2.89	48.0	b.d.l.	b.d.l.	1.39	b.d.l.	11.1	99.4
			S.D. pristine		0.4	0.13	0.5			0.02		0.1	1.0
			avg. altered	0.40	1.76	5.24	43.4	b.d.l.	0.45	2.26	b.d.l.	17.4	71.7
			S.D. altered	0.04	0.18	0.42	3.2		0.22	0.10		1.5	5.4
LK06-0104	LK	CL+CP	avg. pristine	b.d.l.	34.5	0.58	49.6	b.d.l.	b.d.l.	0.58	b.d.l.	13.7	99.6
			S.D. pristine		0.2	0.09	0.2			0.09		0.1	0.5
			avg. altered	0.12	2.16	1.31	49.4	b.d.l.	0.54	2.21	b.d.l.	23.1	78.8
			S.D. altered	0.24	0.75	0.08	6.3		0.04	0.43		3.9	9.7
LK06-0105	LK	CP	avg. pristine	b.d.l.	39.5	4.32	41.8	b.d.l.	b.d.l.	3.40	b.d.l.	9.59	98.6
			S.D. pristine		0.2	0.16	0.2			0.11		0.16	0.3
			Altered	0.65	1.03	6.03	56.9	b.d.l.	0.94	0.67	b.d.l.	6.36	72.5
LK06-0106	LK	CL	pristine	b.d.l.	31.3	1.27	47.9	b.d.l.	b.d.l.	1.32	b.d.l.	16.0	98.2
			avg. altered	b.d.l.	1.69	2.31	47.8	b.d.l.	0.36	2.22	b.d.l.	25.8	81.1
			S.D. altered		0.31	0.17	0.6		0.05	0.13		2.1	2.2
LK06-0107	LK	CL	avg. pristine	b.d.l.	29.3	2.76	49.3	b.d.l.	b.d.l.	3.34	b.d.l.	14.6	99.3
			avg. altered	b.d.l.	2.80	4.16	43.7	b.d.l.	0.51	2.20	b.d.l.	15.6	69.5
			S.D. altered		2.35	0.31	6.4		0.17	0.26		1.1	10.0
LK06-0108	LK	CP	avg. pristine	b.d.l.	30.4	1.89	48.3	b.d.l.	b.d.l.	1.50	b.d.l.	16.8	99.4
			avg. altered	b.d.l.	2.08	3.38	50.4	b.d.l.	0.53	1.75	b.d.l.	21.9	80.3
			S.D. altered		0.71	0.18	3.0		0.06	0.16		0.6	2.5
LK06-0109	LK	CL	avg. pristine	b.d.l.	28.5	3.24	48.5	b.d.l.	b.d.l.	2.77	b.d.l.	15.5	98.7
			S.D. pristine		0.2	0.15	0.3			0.04		0.2	0.7
			avg. altered	b.d.l.	4.29	5.47	46.9	b.d.l.	0.45	1.97	b.d.l.	16.2	76.5
			S.D. altered		0.10	0.29	1.5		0.11	0.04		0.2	1.4
LK06-0110	LK	CL	avg. pristine	b.d.l.	30.5	0.18	46.2	b.d.l.	b.d.l.	0.48	b.d.l.	20.5	99.6
			S.D. pristine		0.1	0.31	0.1			0.06		0.2	0.8
			avg. altered	b.d.l.	4.55	1.26	43.7	b.d.l.	0.29	1.57	b.d.l.	28.7	81.7
			S.D. altered		0.89	0.22	1.9		0.05	0.13		1.8	3.1
LK06-0111	LK	CP	avg. pristine	b.d.l.	34.6	3.89	49.8	b.d.l.	b.d.l.	2.64	b.d.l.	8.5	99.7
			S.D. pristine		0.2	0.43	0.5			0.02		0.2	0.9
			avg. altered	b.d.l.	0.44	5.71	72.7	b.d.l.	b.d.l.	2.31	b.d.l.	2.6	83.8
			S.D. altered		0.03	0.20	1.2			0.15		0.3	1.3
LK06-0021	LK	CP	avg. pristine	b.d.l.	35.5	2.92	47.4	b.d.l.	b.d.l.	2.17	b.d.l.	11.8	99.9
			S.D. pristine		0.2	0.11	0.2			0.10		0.1	0.4

			avg. altered	0.22	0.41	5.83	56.3	b.d.l.	0.04	2.33	0.06	6.25	71.6
			S.D. altered	0.20	0.31	0.25	3.1		0.09	0.14	0.14	1.76	2.8
LK06-0112	LK	CL + CP	avg. pristine	b.d.l.	34.4	0.60	50.3	b.d.l.	b.d.l.	0.76	b.d.l.	13.4	99.6
			S.D. pristine		0.2	0.03	0.5			0.06		0.2	0.6
			avg. altered	b.d.l.	0.81	2.01	49.4	b.d.l.	b.d.l.	3.77	b.d.l.	24.7	81.0
			S.D. altered		0.12	1.18	2.5			0.31		1.1	3.9
LK06-0113	LK	CL + CP	avg. pristine	b.d.l.	31.2	2.13	44.9	b.d.l.	b.d.l.	3.56	b.d.l.	17.4	99.5
			S.D. pristine		0.4	0.04	0.8			0.19		0.2	1.5
			avg. altered	b.d.l.	0.88	4.01	44.9	b.d.l.	0.15	3.40	b.d.l.	21.3	74.9
			S.D. altered		0.35	0.62	1.7		0.17	0.17		1.6	3.2
LK06-0036	LK	CP	avg. pristine	b.d.l.	25.6	3.13	48.8	b.d.l.	b.d.l.	6.44	b.d.l.	15.7	99.6
			S.D. pristine		0.2	0.23	0.4			0.01		0.1	0.7
			avg. altered	0.23	0.93	4.36	46.4	b.d.l.	b.d.l.	3.00	0.04	13.6	69.5
			S.D. altered	0.29	0.47	0.46	3.0			0.87	0.13	5.9	7.3
LK06-0114	LK	CP	avg. pristine	b.d.l.	32.0	2.47	49.3	b.d.l.	b.d.l.	2.29	b.d.l.	12.7	99.6
			S.D. pristine		0.1	0.04	0.1			0.17		0.3	0.1
			avg. altered	b.d.l.	2.14	4.20	46.6	b.d.l.	0.11	3.55	b.d.l.	17.1	74.3
			S.D. altered		1.57	0.13	2.2		0.19	0.21		0.6	3.0
LK06-0046	LK	CP	avg. pristine	b.d.l.	29.8	3.30	43.1	b.d.l.	b.d.l.	3.07	b.d.l.	20.0	99.2
			S.D. pristine		0.1	0.15	0.2			0.05		0.1	0.1
			avg. altered	0.04	1.96	5.08	44.0	0.28	0.23	2.70	b.d.l.	20.6	75.3
			S.D. altered	0.11	1.47	0.37	2.4	0.45	0.24	0.44		4.6	6.1
LK06-0115	LK	CP	avg. pristine	b.d.l.	30.1	2.99	46.1	b.d.l.	b.d.l.	2.53	b.d.l.	17.4	99.9
			S.D. pristine		0.6	0.27	1.2			0.19		2.1	0.5
			avg. altered	0.10	2.50	4.61	43.8	b.d.l.	b.d.l.	2.02	0.07	13.0	67.1
			S.D. altered	0.22	0.95	0.60	5.2			0.10	0.15	1.8	4.8
LK06-0116	LK	CL	avg. pristine	b.d.l.	37.0	1.73	46.5	b.d.l.	b.d.l.	2.18	b.d.l.	12.7	100.2
			S.D. pristine		0.0	0.09	0.2			0.09		0.1	0.6
			avg. altered	b.d.l.	4.73	3.84	45.2	b.d.l.	0.06	3.09	0.17	14.1	73.0
			S.D. altered		1.86	1.09	6.8		0.13	0.40	0.19	0.7	11.4
LK06-0051	LK	CP	avg. pristine	b.d.l.	36.9	2.13	44.8	b.d.l.	b.d.l.	2.08	b.d.l.	14.3	100.3
			S.D. pristine		0.2	0.09	0.0			0.05		0.3	0.1
			avg. altered	0.03	0.61	3.86	50.6	0.35	0.13	1.79	b.d.l.	7.74	66.0
			S.D. altered	0.10	0.83	0.46	6.1	0.84	0.20	0.15		3.29	6.8

LK06-0117	LK	CP	avg. pristine	b.d.l.	32.8	2.95	41.4	b.d.l.	b.d.l.	2.47	b.d.l.	19.4	99.3
			S.D. pristine		0.1	0.24	0.4			0.01		0.0	0.3
			avg. altered	b.d.l.	0.89	4.83	40.3	0.05	0.07	2.65	0.08	18.3	69.7
			S.D. altered		0.74	0.91	6.9	0.16	0.13	0.35	0.15	4.7	10.5
18.01	MB	CP	avg. pristine	b.d.l.	39.2	3.76	52.4	b.d.l.	b.d.l.	3.68	b.d.l.	1.52	100.7
			S.D. pristine		0.5	0.06	0.6			0.09		0.06	1.1
			avg. altered	b.d.l.	0.44	2.76	80.5	0.00	0.12	0.50	b.d.l.	0.42	84.7
			S.D. altered		0.15	0.24	4.6	0.00	0.17	0.08		0.14	4.9
18.02	MB	CP	pristine	b.d.l.	19.9	2.32	52.3	1.22	b.d.l.	1.44	b.d.l.	11.8	89.7
			avg. altered	0.15	0.15	1.36	55.6	8.91	2.30	0.41	b.d.l.	11.4	80.6
			S.D. altered	0.18	0.29	1.01	25.5	11.40	2.90	0.78		12.7	5.2
18c.21	MB	CP	avg. pristine	b.d.l.	30.9	2.65	46.9	b.d.l.	b.d.l.	1.30	b.d.l.	17.4	99.5
			S.D. pristine		0.2	0.12	0.5			0.11		0.2	0.9
			avg. altered	b.d.l.	0.56	1.66	71.3	1.59	0.30	b.d.l.	b.d.l.	5.66	81.1
			S.D. altered		0.61	0.44	3.1	0.44	0.30			0.71	3.1
18c.22	MB	CP	avg. pristine	b.d.l.	24.0	2.82	46.7	b.d.l.	b.d.l.	4.66	b.d.l.	20.2	98.4
			S.D. pristine		0.5	0.07	1.5			0.76		0.4	0.3
			avg. altered	0.10	0.62	1.29	73.1	1.67	0.29	0.14	b.d.l.	7.40	84.6
			S.D. altered	0.18	0.56	0.43	5.2	0.44	0.24	0.41		0.96	3.8
21.65	MB	CP	avg. pristine	b.d.l.	32.7	2.78	47.3	b.d.l.	b.d.l.	3.55	b.d.l.	12.7	99.1
			S.D. pristine		0.1	0.07	0.2			0.10		0.1	0.2
			avg. altered	0.65	0.33	3.39	60.4	1.13	0.95	b.d.l.	b.d.l.	5.89	72.9
			S.D. altered	0.20	0.26	0.26	4.4	0.11	0.31			0.41	4.5
21p.06	MB	CP	avg. pristine	b.d.l.	30.6	3.87	44.1	b.d.l.	b.d.l.	3.46	b.d.l.	16.4	98.7
			S.D. pristine		0.3	0.20	0.4			0.04		0.3	0.6
			avg. altered	0.66	0.19	5.32	59.5	1.62	1.17	b.d.l.	0.21	5.07	73.7
			S.D. altered	0.17	0.16	1.20	5.9	0.52	0.32		0.22	1.88	5.7
7b.100	PT	CP	avg. pristine	b.d.l.	38.5	3.77	47.4	b.d.l.	b.d.l.	3.98	b.d.l.	5.76	99.6
			S.D. pristine		0.3	0.28	0.2			0.10		0.16	0.6
			avg. altered	0.29	1.48	3.77	55.7	0.64	0.69	0.84	b.d.l.	3.53	67.0
			S.D. altered	0.25	1.72	0.96	13.6	0.18	0.31	0.42		0.98	12.4
7b.101	PT	CP	avg. pristine	b.d.l.	39.5	9.43	40.8	b.d.l.	b.d.l.	8.51	0.53	0.87	99.7
			S.D. pristine		0.7	0.05	0.2			0.22	0.02	0.05	0.6
			avg. altered	0.32	0.61	6.26	54.9	0.18	1.13	1.06	0.68	0.63	65.7

			S.D. altered	0.07	0.03	0.91	4.1	0.32	0.13	0.11	0.05	0.31	4.5
7bis.04	PT	CP	avg. pristine	b.d.l.	41.1	2.65	45.0	b.d.l.	b.d.l.	2.91	b.d.l.	6.27	98.0
			S.D. pristine		2.9	0.35	0.4			0.30		0.02	3.3
			avg. altered	0.19	0.56	4.67	52.6	1.11	0.68	1.09	0.04	6.50	67.5
			S.D. altered	0.16	0.15	0.62	6.9	0.63	0.12	0.17	0.11	0.90	7.6
7bis.05	PT	CP	avg. pristine	b.d.l.	33.6	4.10	47.0	b.d.l.	b.d.l.	3.77	0.07	10.8	99.4
			S.D. pristine		4.2	0.13	0.4			0.20	0.16	4.2	0.6
			avg. altered	0.10	0.55	4.95	71.2	0.84	0.49	0.78	0.23	2.79	81.9
			S.D. altered	0.18	0.07	0.43	2.1	0.10	0.08	0.15	0.20	0.26	1.2
7bis.06	PT	CL	avg. pristine	b.d.l.	40.6	3.41	52.1	b.d.l.	b.d.l.	3.52	b.d.l.	0.93	100.5
			S.D. pristine		0.1	0.09	0.0			0.01		0.06	0.1
			avg. altered	0.61	1.22	4.60	68.7	b.d.l.	0.39	b.d.l.	b.d.l.	1.27	76.8
			S.D. altered	0.10	0.13	0.23	2.7		0.03			0.17	2.7
7.4	PT	CP	avg. pristine	b.d.l.	33.3	3.46	42.0	b.d.l.	b.d.l.	3.07	0.16	16.2	98.3
			S.D. pristine		0.1	0.03	0.1			0.03	0.22	0.1	0.3
			avg. altered	0.21	0.38	2.79	66.6	1.74	0.37	0.23	0.22	5.66	78.3
			S.D. altered	0.22	0.34	0.81	5.0	1.01	0.40	0.66	0.19	4.42	6.1
7.41	PT	CP	avg. pristine	b.d.l.	39.7	3.35	48.9	b.d.l.	b.d.l.	1.38	b.d.l.	6.54	100.3
			S.D. pristine		0.2	0.25	0.2			0.05		0.14	0.5
			avg. altered	0.32	0.27	3.62	72.0	0.84	0.34	b.d.l.	0.20	2.38	80.0
			S.D. altered	0.39	0.26	0.92	4.8	0.24	0.28		0.18	0.48	6.0

avg, = averages.

S.D. = Standard deviation.

b.d.l. = below detection limit.

[a] LK = Larkman Nunatak; MB = Miller Butte; PT = Pian delle Tectiti.

[b] Type of weathering (explained in the text): CP = corrosion pits; CL = continuous layer.

Table 5. Representative WDS analyses of metal droplets in cosmic spherules from the Larkman nunatak (in wt%).

	Type	S	Fe	Ni	Co	Total	Fe/Ni[a]
LK06-0076	BO	b.d.l.	84.2	12.2	b.d.l.	96.4	7.3
LK06-0059	BO	b.d.l.	60.7	35.9	b.d.l.	96.6	1.8
LK06-0085	BO	b.d.l.	54.4	40.4	b.d.l.	94.8	1.4
LK06-0085	BO	34.8	40.1	24.8	b.d.l.	99.9	
LK06-0067	Po	b.d.l.	41.8	53.2	3.9	98.9	0.8
LK06-0067	Po	34.9	30.4	35.2	b.d.l.	100.5	
LK06-0083	Po	35.2	30.9	33.9	b.d.l.	100.0	
LK06-0074	V	b.d.l.	85.4	10.7	b.d.l.	96.5	8.4
LK06-0044	BO	b.d.l.	78.2	18.8	b.d.l.	97.1	4.4
LK06-0082	C	b.d.l.	62.6	35.4	b.d.l.	98.0	1.9
LK06-0086	C	b.d.l.	71.6	23.2	b.d.l.	94.2	3.3

[a] Atomic ratios

b.d.l. = below detection limit.

Table 6. Representative WDS analyses of weathering products of metal droplets in cosmic spherules from the Larkman nunatak (in oxide wt%).

	Type	Na_2O	MgO	Al_2O_3	SiO_2	P_2O_5	SO_3	Cl	K_2O	CaO	Fe_2O_3	NiO	Total	Fe/Ni[a]
LK06-0076	BO	b.d.l.	b.d.l.	1.81	4.98	b.d.l.	4.59	1.08	b.d.l.	0.85	62.7	3.26	79.3	18.0
LK06-0059	BO	b.d.l.	b.d.l.	2.04	9.20	b.d.l.	9.44	0.26	b.d.l.	0.78	59.0	6.95	87.7	7.9
LK06-0085	BO	0.65	0.80	3.78	6.85	1.49	7.59	0.26	b.d.l.	1.43	47.5	8.72	79.0	5.0
LK06-0067	PO	b.d.l.	0.66	2.93	10.3	b.d.l.	6.94	0.90	0.43	1.18	50.3	8.47	82.2	5.5
LK06-0083	PO	b.d.l.	b.d.l.	5.69	9.50	1.10	9.79	0.31	b.d.l.	1.78	54.3	0.94	83.5	53.7
LK06-0074	V	b.d.l.	0.50	3.08	9.71	b.d.l.	5.09	0.32	b.d.l.	1.12	57.6	2.30	79.7	34.8
LK06-0087	C	b.d.l.	b.d.l.	4.33	4.02	1.51	4.82	b.d.l.	b.d.l.	1.09	58.5	3.93	78.2	13.2
LK06-0082	C	b.d.l.	b.d.l.	7.09	6.33	1.15	5.87	0.28	b.d.l.	1.80	58.7	1.78	83.0	30.7
LK06-0086	C	b.d.l.	b.d.l.	0.51	4.09	b.d.l.	7.47	0.21	b.d.l.	0.00	70.0	6.11	88.4	10.7

[a] Atomic ratios

b.d.l. = below detection limit.

Table 7. Major element composition of secondary phases in G-type cosmic spherule #LK06-0027 (data in oxide wt%)

	core		crack		encrustation	
	avg (n=3)	S.D.	avg (n=3)	S.D.	avg (n=3)	S.D.
Na_2O	0.59	0.09	b.d.l.	b.d.l.	0.19	0.33
MgO	0.15	0.27	0.88	0.05	b.d.l.	b.d.l.
Al_2O_3	2.59	0.45	3.33	1.69	2.14	0.33
SiO_2	5.33	0.55	7.22	2.92	5.26	0.58
P_2O_5	b.d.l.	b.d.l.	0.39	0.67	b.d.l.	b.d.l.
SO_3	4.01	0.34	3.29	0.95	5.72	0.62
Cl	0.21	0.19	0.07	0.12	0.39	0.13
CaO	0.77	0.13	1.06	0.19	0.71	0.07
Fe_2O_3	68.5	2.9	70.2	2.9	62.3	1.4
NiO	3.42	0.16	2.59	0.38	2.05	0.99
Total	85.5		89.1		78.8	

avg = average.
S.D. = standard deviation.
b.d.l. = below detection limit.
n= number of analyses.

Table 8. Results of mass balance calculation between original and altered glass in V-type and Po cosmic spherules.

Particle	ToW[a]	Na_2O (wt%)	MgO (wt%)	(%)[b]	Al_2O_3 (wt%)	(%)	SiO_2 (wt%)	(%)	K_2O (wt%)	CaO (wt%)	(%)	TiO_2 (wt%)	FeO (wt%)	(%)
V-type cosmic spherules														
Larkman Nunatak														
LK06-0098	CL	0.73	-29.9	-94	0.29	14	-11.7	-25	0.12	-0.27	-21	-	-1.57	-9
LK06-0063	CP	0.44	-36.4	-94	0.42	18	-15.4	-29	0.27	-0.94	-42	-	0.84	19
LK06-0066	CL	0.15	-31.2	-96	0.59	44	-14.0	-28	0.21	0.33	24	-	2.49	18
LK06-0099	CL	0.68	-25.3	-95	0.73	36	-13.8	-26	0.13	-7.99	-82	0.35	2.77	27
LK06-0100	CL	-	-29.7	-96	1.17	55	-11.5	-25	0.46	-1.18	-42	0.07	2.28	13
LK06-0075	CL + CP	0.32	-30.8	-97	0.79	29	-8.0	-18	0.41	-1.23	-58	-	-5.43	-33
LK06-0101	CL	0.35	-28.9	-96	1.07	34	-9.2	-19	0.74	-0.18	-11	-	-2.71	-17
LK06-0102	CL	0.27	-26.6	-95	0.19	12	-21.4	-41	0.03	-2.43	-66	0.05	-1.62	-12
LK06-0103	CL	0.30	-34.4	-96	0.99	34	-15.9	-33	0.33	0.28	20	-	1.78	16
LK06-0105	CP	0.48	-38.7	-98	0.15	3	0.3	1	0.70	-2.90	-85	-	-4.88	-51
LK06-0106	CL	-	-30.0	-96	0.44	35	-12.5	-26	0.27	0.32	25	-	3.07	19
LK06-0107	CL	-	-27.2	-93	0.32	12	-16.9	-34	0.38	-1.71	-51	-	-3.04	-21
LK06-0108	CP	-	-28.9	-95	0.61	32	-11.0	-23	0.39	-0.20	-14	-	-0.55	-3
LK06-0109	CL	-	-25.3	-89	0.81	25	-13.8	-28	0.33	-1.31	-47	-	-3.50	-23
LK06-0111	CP	-	-34.3	-99	0.34	9	4.1	8	-	-0.93	-35	-	-6.58	-77
LK06-0021	CP	0.16	-35.2	-99	1.40	48	-5.7	-12	0.03	-0.44	-20	0.04	-7.21	-61
LK06-0113	CL + CP	-	-30.5	-98	0.84	39	-11.6	-26	0.11	-1.04	-29	-	-1.55	-9
LK06-0036	CP	0.17	-24.9	-97	0.10	3	-14.4	-30	-	-4.22	-65	0.03	-5.61	-36
LK06-0114	CP	-	-30.4	-95	0.64	26	-14.8	-30	0.08	0.34	15	-	-0.03	0
LK06-0046	CP	0.03	-28.3	-95	0.46	14	-10.5	-24	0.17	-1.07	-35	-	-4.75	-24
LK06-0115	CP	0.07	-28.2	-94	0.42	14	-13.7	-30	-	-1.03	-41	0.05	-7.80	-45
LK06-0116	CL	-	-33.5	-91	1.11	64	-13.0	-28	0.04	0.11	5	0.13	-2.20	-17
LK06-0051	CP	0.02	-36.4	-99	0.73	34	-7.3	-16	0.10	-0.75	-36	-	-8.55	-60
LK06-0117	CP	-	-32.1	-98	0.63	21	-11.5	-28	0.05	-0.51	-21	0.06	-5.85	-30
Transantarctic Mountains														
18.01	CP	-	-38.9	-99	-1.72	-46	7.2	14	0.09	-3.31	-90	-	-1.21	-80
18.02	CP	0.11	-19.8	-99	-1.31	-57	-11.1	-21	1.70	-1.14	-79	-	-3.39	-29

18c.21	CP	-	-30.5	-99	-1.42	-54	5.9	13	0.22	-1.30	-100	-	-13.25	-76
18c.22	CP	0.07	-23.5	-98	-1.86	-66	7.4	16	0.21	-4.56	-98	-	-14.72	-73
21.65	CP	0.48	-32.5	-99	-0.27	-10	-2.6	-5	0.70	-3.55	-100	-	-8.38	-66
7b.100	CP	0.21	-37.4	-97	-0.98	-26	-6.1	-13	0.51	-3.36	-84	-	-3.15	-55
7b.101	CP	0.24	-39.0	-99	-4.79	-51	-0.1	0	0.84	-7.72	-91	-0.03	-0.40	-46
7bis.04	CP	0.14	-40.7	-99	0.81	31	-6.0	-13	0.50	-2.10	-72	0.03	-1.46	-23
7bis.05	CP	0.07	-33.2	-99	-0.43	-11	5.7	12	0.36	-3.19	-85	0.10	-8.76	-81
7bis.06	CL	0.45	-39.7	-98	0.00	0	-1.2	-2	0.29	-3.52	-100	-	0.01	1
7.4	CP	0.16	-33.0	-99	-1.39	-40	7.3	17	0.27	-2.90	-94	0.00	-12.06	-74
7.41	CP	0.24	-39.5	-99	-0.67	-20	4.4	9	0.25	-1.38	-100	0.15	-4.78	-73
Po cosmic spherules														
7.42		-	-2.4	-88	-5.66	-67	-8.0	-18	-	-6.94	-95	-0.11	-21.13	-60
21.65		0.30	-1.0	-57	-4.35	-58	-4.5	-10	0.70	-9.89	-100	0.39	-26.55	-73
LK06-0050		-	-1.1	-53	-1.45	-32	-12.2	-32	-	-17.11	-91	0.07	-14.96	-44
LK06-0018		-	-3.7	-43	-2.94	-53	-12.3	-32	0.18	-10.27	-68	0.27	-8.22	-32

[a] Type of weathering (explained in the text): CP = corrosion pits; CL = continuous layer

[b] Results are both in wt% and % for elements that are present in the pristine glass and its alteration product.

Table 9. Major element compositions of pristine and altered glass in 4 Po cosmic spherules (data in wt%).

Sample	Locality[a]	n		SiO_2	TiO_2	Al_2O_3	Cr_2O_3	FeO	MnO	MgO	CaO	Na_2O	K_2O	SO_3	P_2O_5	Total
7.42	MB	4	avg. pristine	44.3	0.49	8.42	0.10	35.2	0.37	2.68	7.34	b.d.l.	b.d.l.	b.d.l.	b.d.l.	98.9
			S.D. pristine	1.6	0.04	0.06	0.20	1.6	0.25	0.53	0.23					0.4
		3	avg. altered	49.0	0.51	3.73	0.09	19.0	b.d.l.	0.43	0.54	b.d.l.	b.d.l.	0.93	0.14	74.3
			S.D. altered	6.0	0.10	0.55	0.21	6.9		0.46	0.61			0.65	0.32	3.0
21.65	MB	4	avg. pristine	43.4	b.d.l.	7.53	b.d.l.	36.4	0.24	1.74	9.89	b.d.l.	b.d.l.	b.d.l.	0.16	99.3
			S.D. pristine	1.7		1.39		2.8	0.28	0.87	1.06				0.32	0.3
		1	altered	52.5	0.53	4.29	b.d.l.	13.3	b.d.l.	1.01	b.d.l.	0.40	0.95	2.15	b.d.l.	75.2
LK06-0050	LK	4	avg. pristine	38.6	b.d.l.	4.56	b.d.l.	33.7	b.d.l.	2.09	18.86	b.d.l.	b.d.l.	b.d.l.	0.21	98.1
			S.D. pristine	1.9		0.42		0.9		0.19	1.18				0.36	3.1
		4	avg. altered	35.6	0.10	4.20	0.10	25.3	b.d.l.	1.34	2.36	b.d.l.	b.d.l.	0.43	1.26	70.6
			S.D. altered	10.7	0.19	0.56	0.20	11.8		1.41	0.42			0.86	0.79	3.3
LK06-0018	LK	1	pristine	38.3	b.d.l.	5.57	0.50	26.0	0.70	8.67	15.15	b.d.l.	b.d.l.	b.d.l.	b.d.l.	96.0
		1	altered	35.1	0.37	3.55	0.48	24.0	0.57	6.70	6.59	b.d.l.	0.24	1.35	0.55	79.6

avg. = average

S.D. = standard deviation.

b.d.l. = below detection limit.

n = number of analyses.

[a] LK = Larkman Nunatak; MB = Miller Butte.

Table 10. Major element compositions (in oxide wt%) of secondary mineral phases in unmelted coarse-grained micrometeorites #20c.343, #19b.13, #19b.24 and #19b.25.

Particle	n	Comment		Na_2O	MgO	Al_2O_3	SiO_2	P_2O_5	SO_3	Cl	K_2O	CaO	Fe_2O_3	NiO	Total
Jarosite															
19b.13	1			b.d.l.	b.d.l.	0.72	3.6	b.d.l.	27.7	0.47	6.83	b.d.l.	43.2	b.d.l.	82.6
20c.343	7		avg.	0.43	0.28	2.86	3.24	b.d.l.	30.9	b.d.l.	7.91	b.d.l.	37.5	b.d.l.	83.1
			S.D.	0.22	0.35	2.32	3.10		1.5		0.35		2.4		
Alteration products															
19b.13	2	olivine pseudomorphs	avg.	b.d.l.	0.21	1.57	13.9	2.06	5.16	1.55	0.16	0.31	54.2	1.20	80.4
19b.13			S.D.		0.29	0.05	2.10	0.16	0.09	0.07	0.22	0.04	1.0	0.13	
19b.13	1	infilled cavity		b.d.l.	b.d.l.	2.55	6.20	b.d.l.	6.47	1.58	b.d.l.	b.d.l.	62.5	1.86	81.1
19b.13	1	encrustation		b.d.l.	0.10	1.95	4.44	b.d.l.	6.92	1.11	b.d.l.	b.d.l.	64.3	1.83	80.7
19b.24	4	infilled cavity	avg.	b.d.l.	b.d.l.	1.77	5.94	b.d.l.	4.52	b.d.l.	b.d.l.	b.d.l.	63.9	b.d.l.	76.1
			S.D.			1.54	3.64		1.38				4.0		
19b.24	8	encrustation	avg.	b.d.l.	b.d.l.	1.54	1.55	b.d.l.	5.20	1.12	b.d.l.	b.d.l.	66.6	b.d.l.	76.0
			S.D.			1.13	1.43		1.24	0.64			2.1		
19b.25	4	inside particle	avg.	b.d.l.	b.d.l.	2.94	14.1	0.30	9.94	0.85	1.72	0.44	50.5	b.d.l.	80.7
			S.D.			0.63	5.9	0.60	5.61	0.57	1.93	0.87	12.0		
19b.25	9	encrustation	avg.	b.d.l.	b.d.l.	2.15	3.04	b.d.l.	6.43	1.46	b.d.l.	b.d.l.	65.0	b.d.l.	78.1
			S.D.			0.96	1.45		1.21	0.86			2.4		

avg. = average
S.D. = standard deviation.
b.d.l. = below detection limit.
n = number of analyses.

Table 11. Weathering scale for micrometeorites based on the amount of primary material lost and encrustation by secondary material.

Loss and/or alteration of primary material / **Encrusation by secondary material**	Not visible	Minor	Moderate (20-60%)	Severe (>60%)
Not visible	**0a**	**1a**	**2a**	**3a**
Partial	**0b**	**1b**	**2b**	**3b**
Complete	**0c**	**1c**	**2c**	**3c**

Figure 1

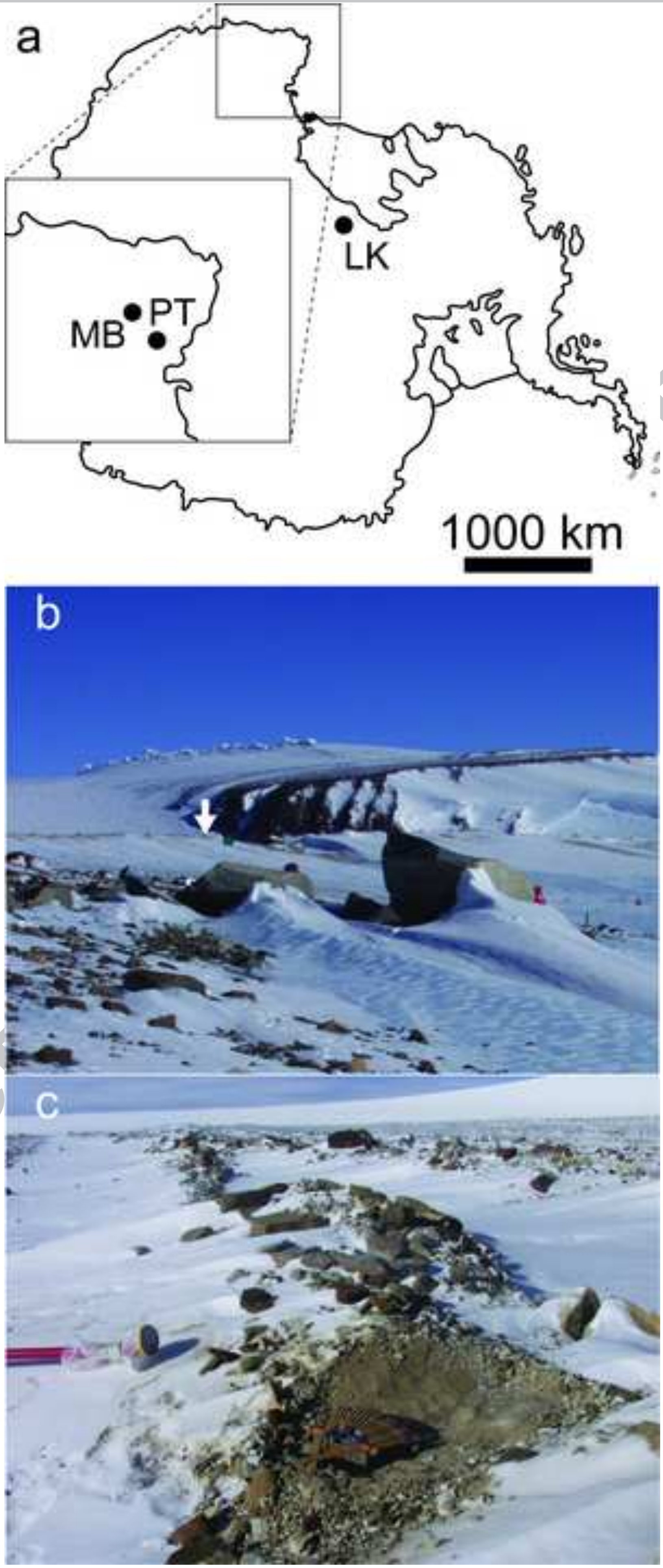

Figure 2

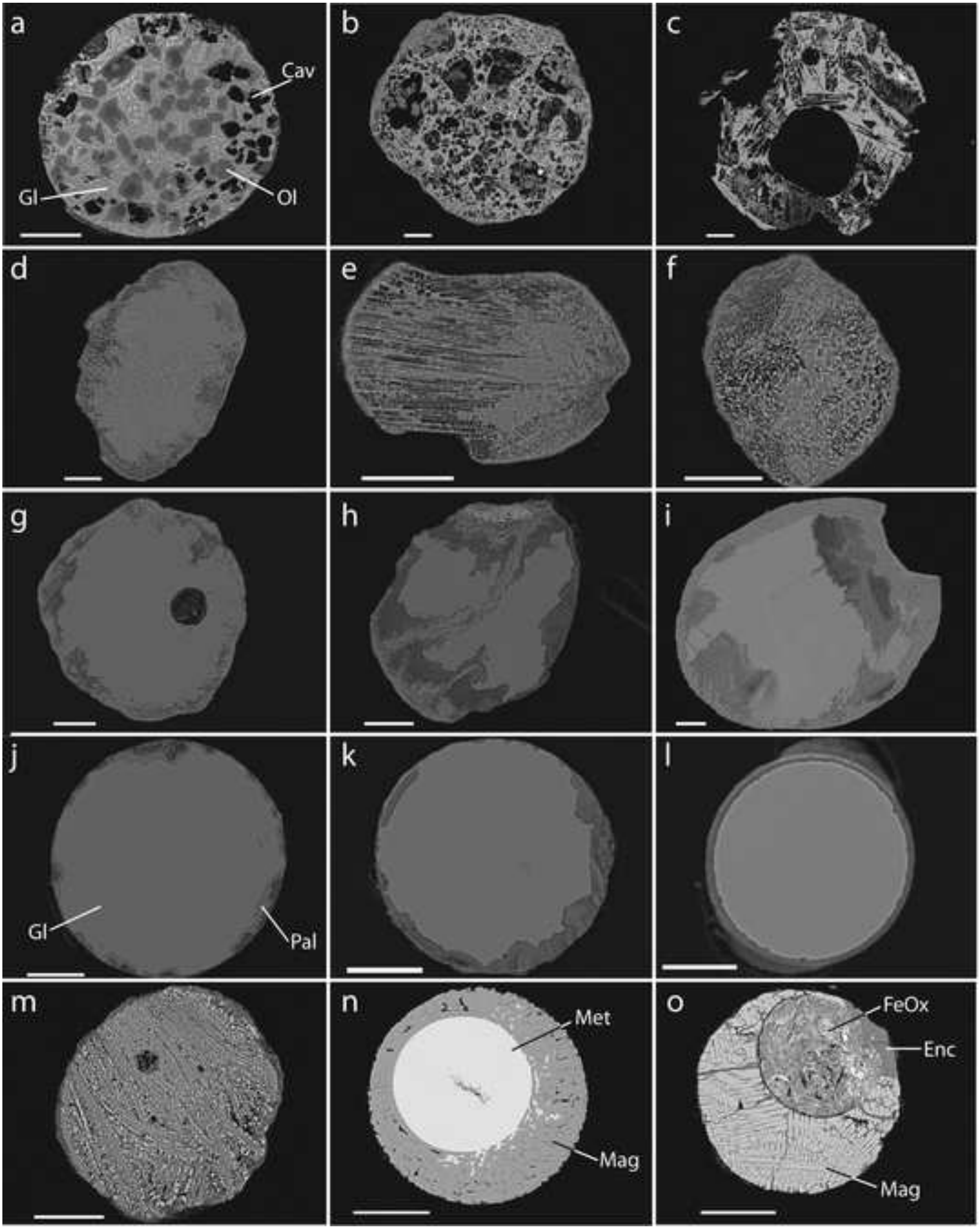

Figure 3

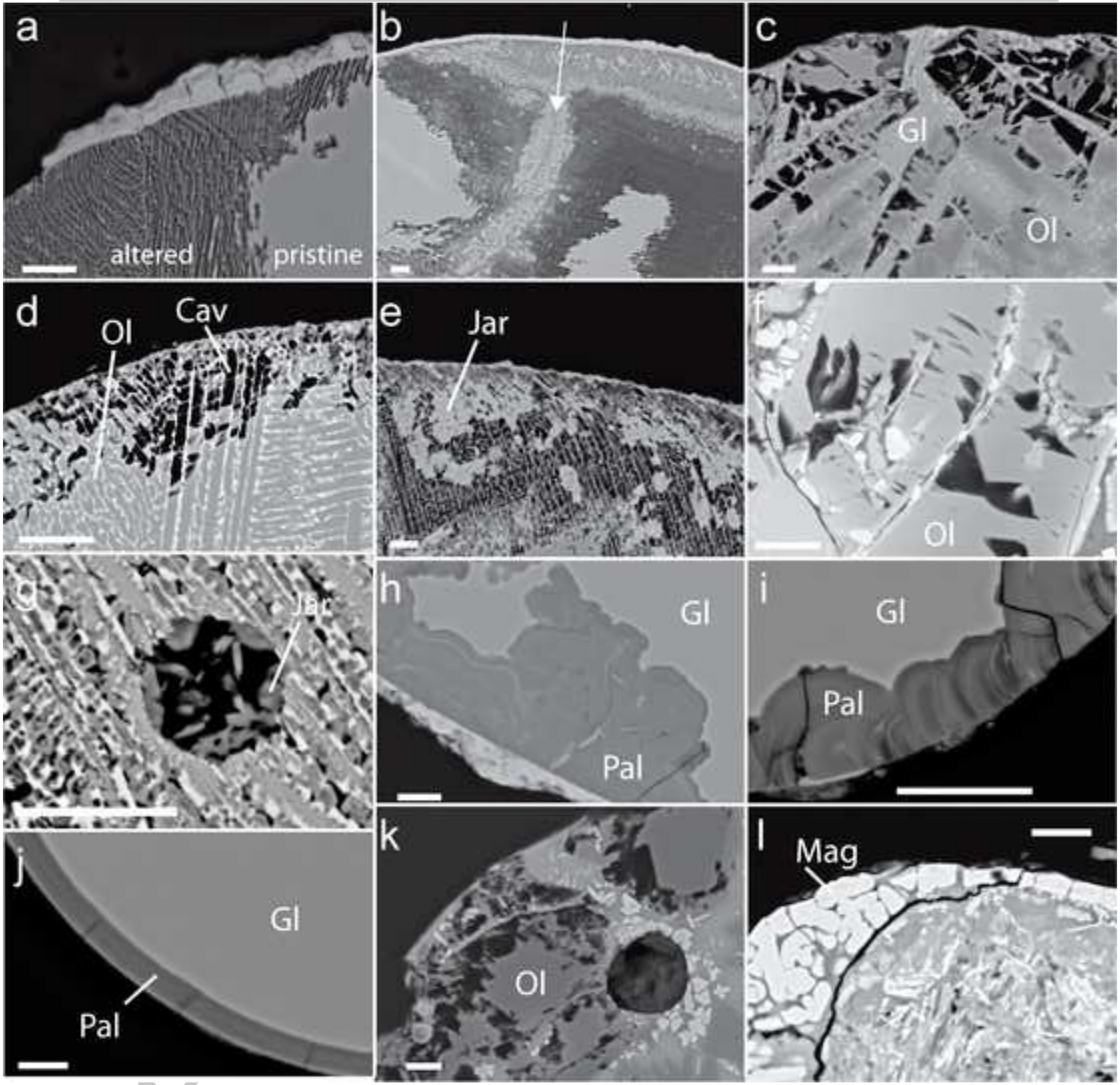
a
altered
pristine
b
c
Gl
Ol
d
Ol
Cav
e
Jar
f
Ol
g
Jar
h
Gl
Pal
i
Gl
Pal
j
Gl
Pal
k
Ol
l
Mag

Figure 4

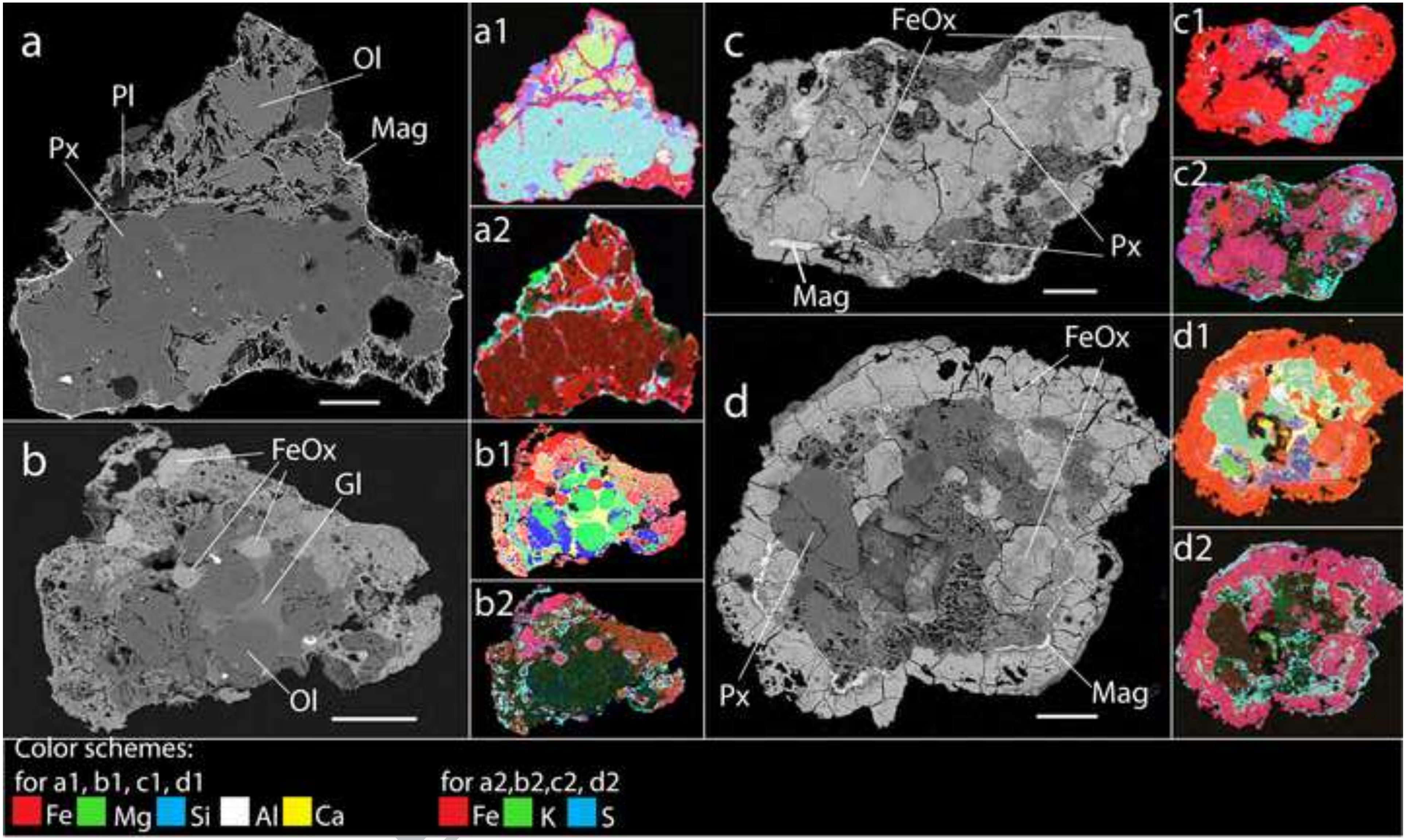
a
Ol
Pl
Mag
Px
a1
a2
b
FeOx
Gl
Ol
b1
b2
c
FeOx
Px
Mag
c1
c2
d
FeOx
Px
Mag
d1
d2
Color schemes:
for a1, b1, c1, d1
Fe Mg Si Al Ca
for a2,b2,c2, d2
Fe K S

Figure 5

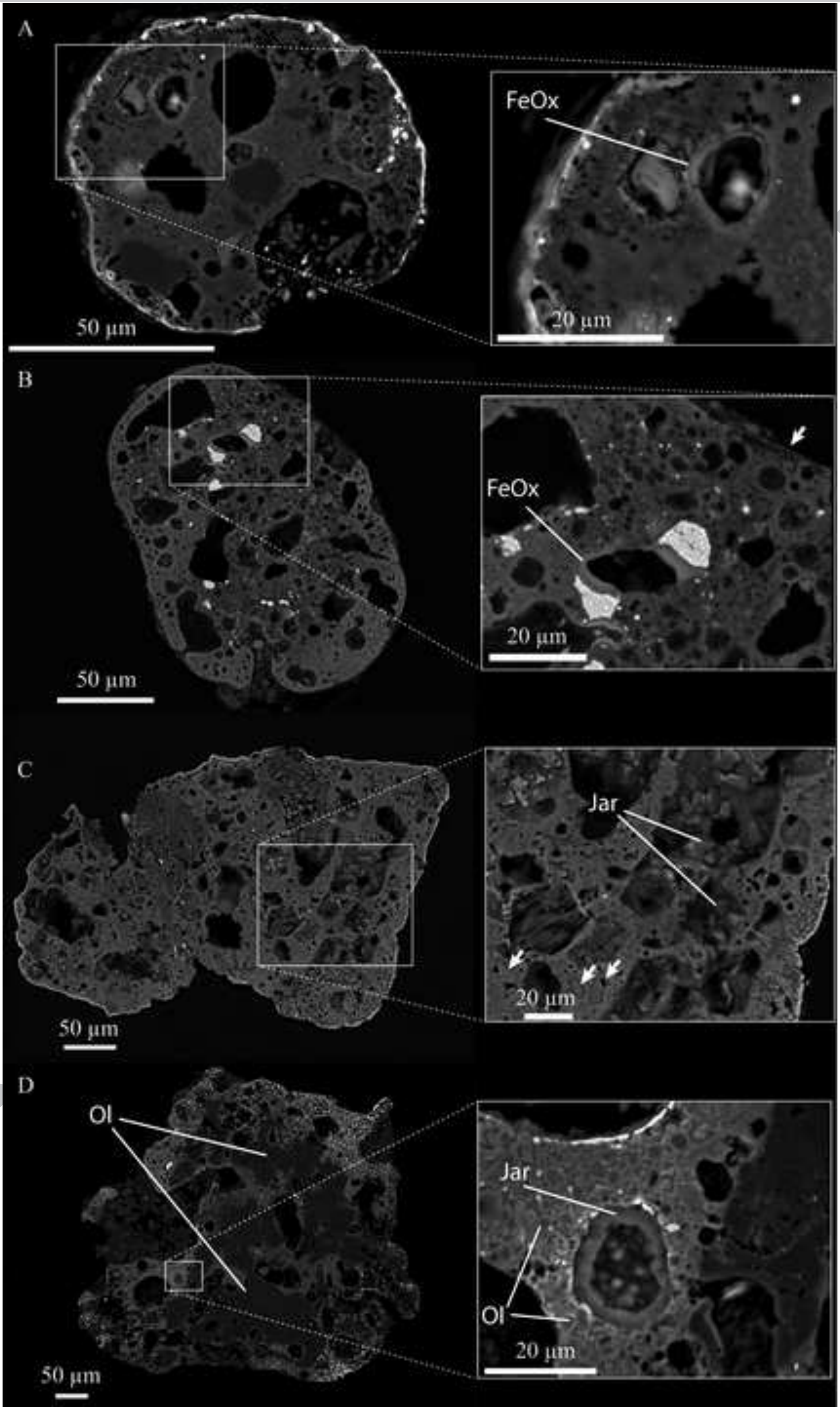
A
FeOx
50 µm
20 µm
B
FeOx
50 µm
20 µm
C
Jar
50 µm
20 µm
D
Ol
Jar
Ol
50 µm
20 µm

Figure 6

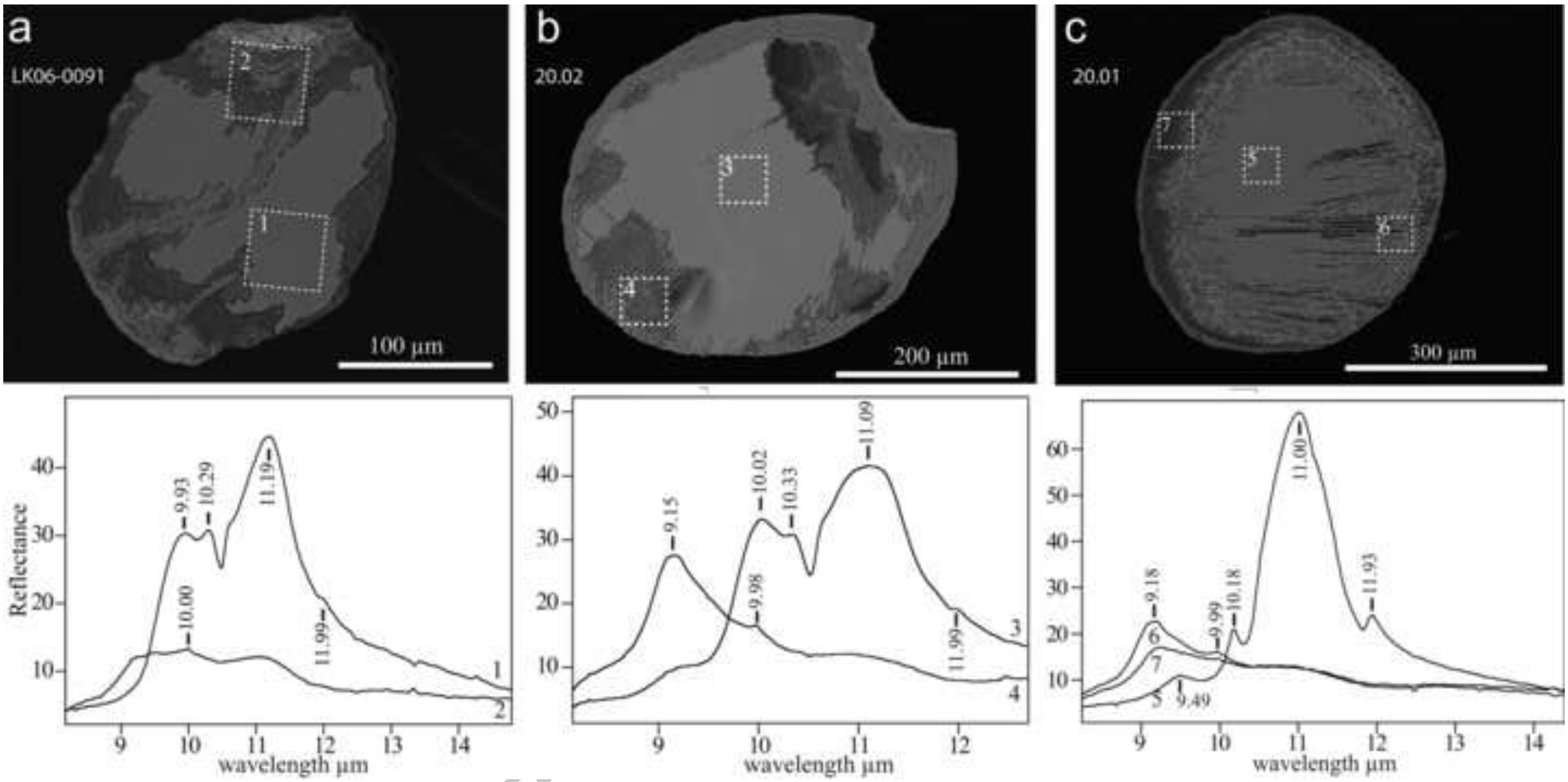
a
LK06-0091
2
1
100 μm
b
20.02
3
4
200 μm
c
20.01
7
5
6
300 μm
Reflectance
wavelength μm
9.93
10.29
11.19
10.00
11.99
1
2
9.15
10.02
10.33
11.09
9.98
11.99
3
4
9.18
9.99
10.18
11.00
11.93
6
7
5
9.49

Figure 7

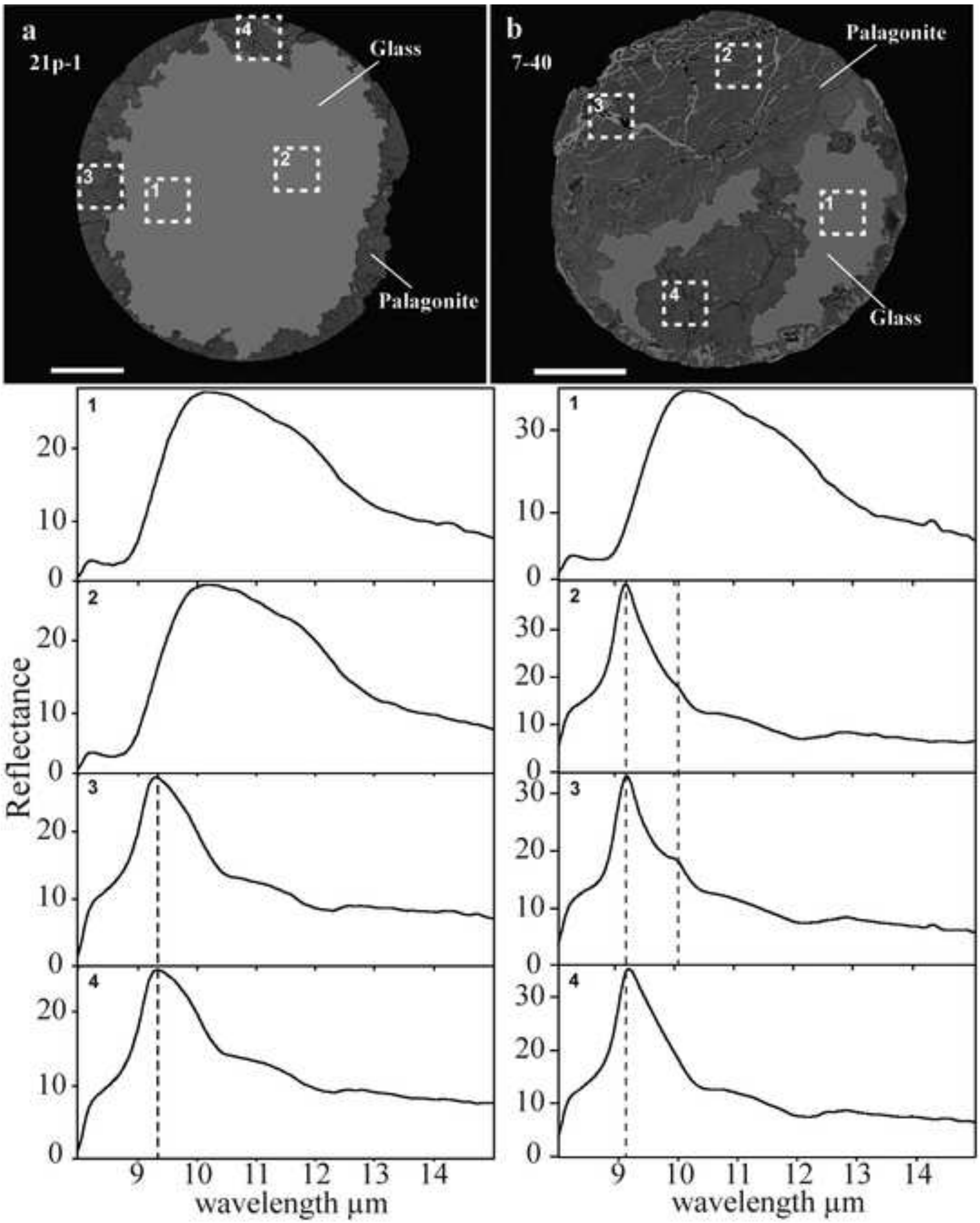
a
21p-1
Glass
Palagonite
b
7-40
Palagonite
Glass
1
2
3
4
Reflectance
wavelength µm
wavelength µm

Figure 8

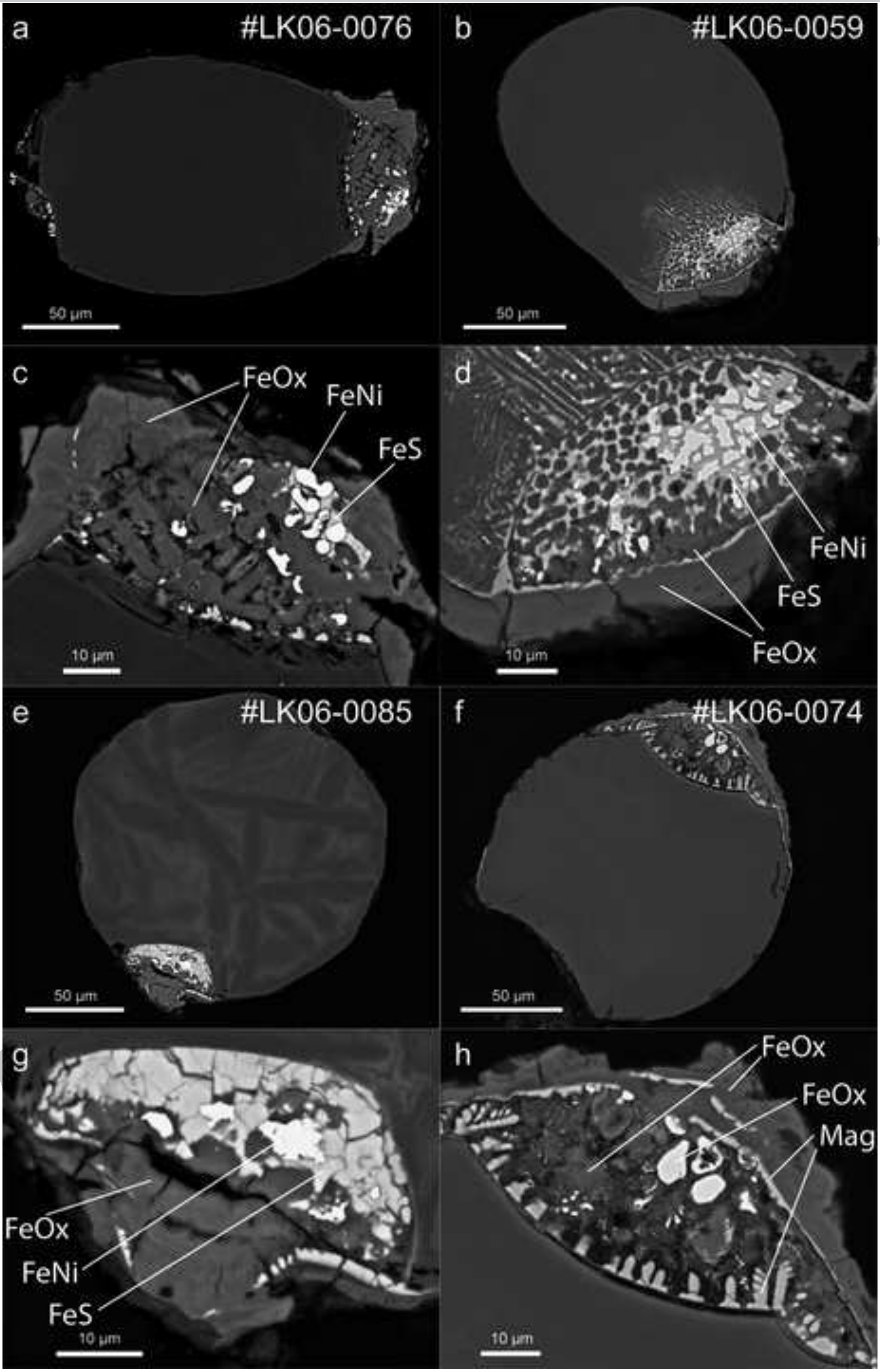
a
#LK06-0076
50 µm
b
#LK06-0059
50 µm
c
FeOx
FeNi
FeS
10 µm
d
FeNi
FeS
FeOx
10 µm
e
#LK06-0085
50 µm
f
#LK06-0074
50 µm
g
FeOx
FeNi
FeS
10 µm
h
FeOx
FeOx
Mag
10 µm

Figure 9

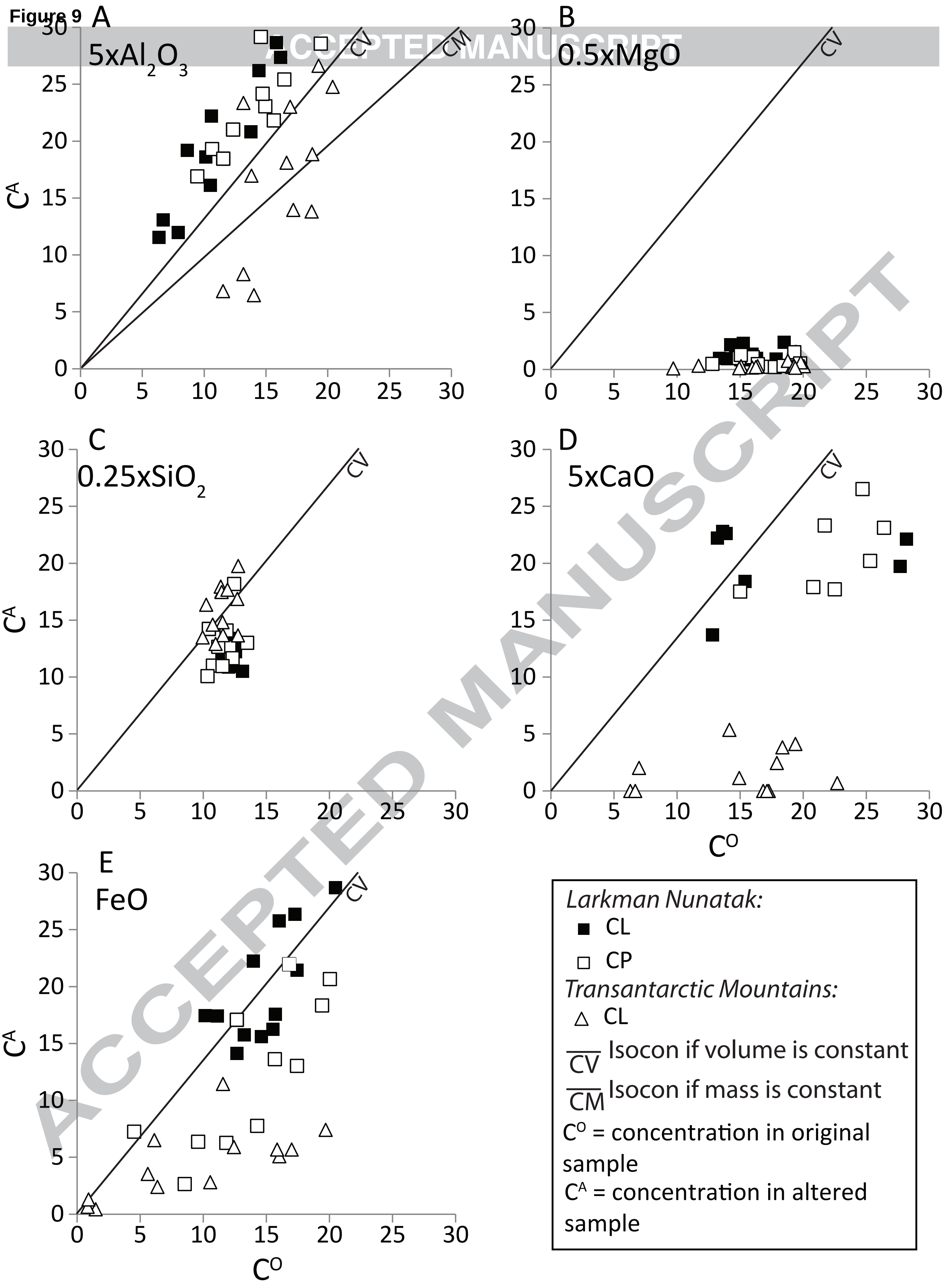
A
5xAl2O3
B
0.5xMgO
C
0.25xSiO2
D
5xCaO
E
FeO
CV
CM
CA
CO
Larkman Nunatak:
CL
CP
Transantarctic Mountains:
CL
CV Isocon if volume is constant
CM Isocon if mass is constant
CO = concentration in original sample
CA = concentration in altered sample

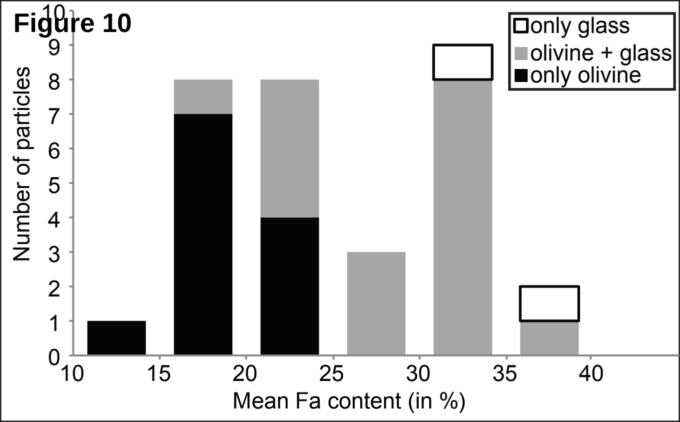

Figure 10
only glass
olivine + glass
only olivine
Number of particles
Mean Fa content (in %)
0
1
2
3
4
5
6
7
8
9
10
10
15
20
25
30
35
40

Figure 11

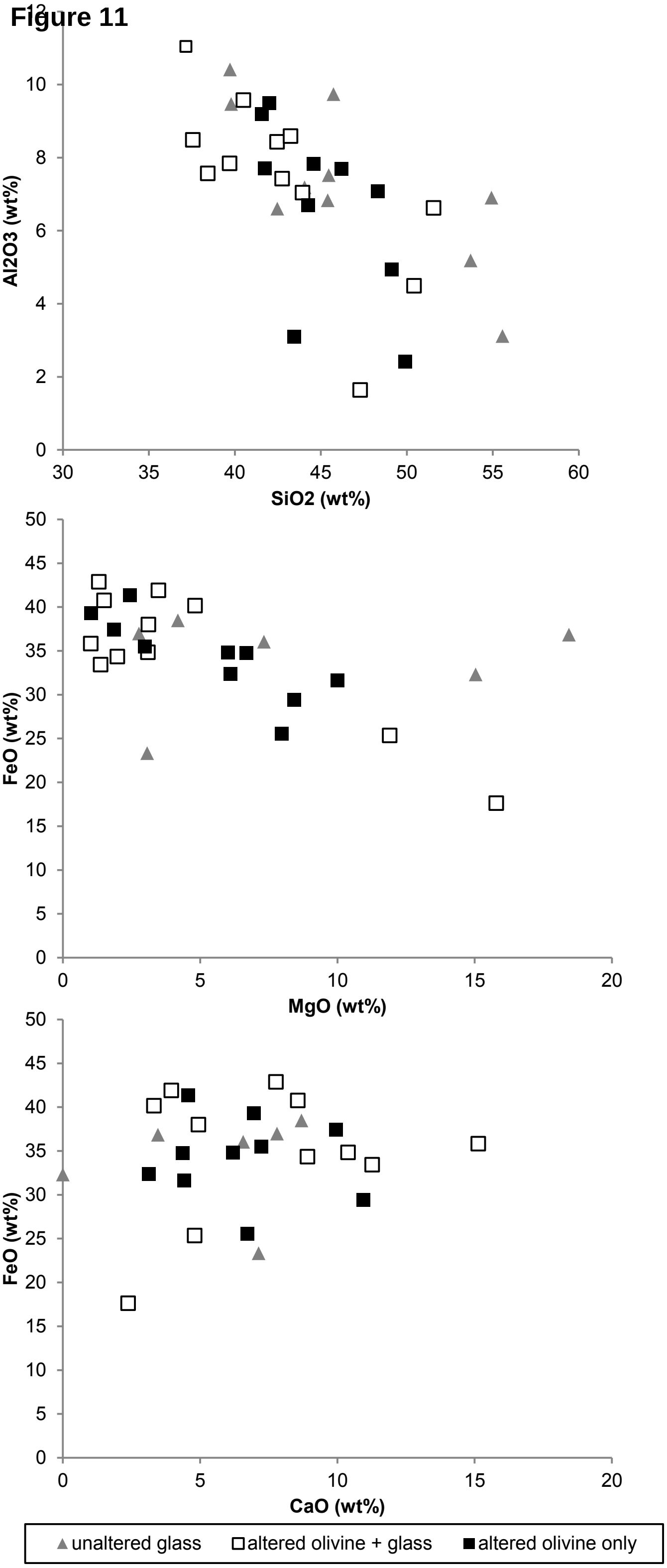

12
10
8
6
4
2
0
Al2O3 (wt%)
30
35
40
45
50
55
60
SiO2 (wt%)
50
45
40
35
30
25
20
15
10
5
0
FeO (wt%)
0
5
10
15
20
MgO (wt%)
50
45
40
35
30
25
20
15
10
5
0
FeO (wt%)
0
5
10
15
20
CaO (wt%)
unaltered glass
altered olivine + glass
altered olivine only